Bioorganic & Medicinal Chemistry 22 (2014) 1751–1765

Contents lists available at ScienceDirect

Bioorganic & Medicinal Chemistry

journal homepage: www.elsevier.com/locate/bmc

Discovery of simplified N^2-substituted pyrazolo[3,4-*d*]pyrimidine derivatives as novel adenosine receptor antagonists: Efficient synthetic approaches, biological evaluations and molecular docking studies

Gopalakrishnan Venkatesan [a], Priyankar Paira [d], Siew Lee Cheong [a], Kosaraju Vamsikrishna [a], Stephanie Federico [b], Karl-Norbert Klotz [c], Giampiero Spalluto [b,*], Giorgia Pastorin [a,*]

[a] Department of Pharmacy, Faculty of Science, National University of Singapore, 3 Science Drive 2, Singapore
[b] Department of Pharmaceutical Sciences, University of Trieste, Piazzale Europa 1, 34128 Trieste, Italy
[c] Institut für Pharmakologie und Toxikologie, Universität Würzburg, D-97078 Würzburg, Germany
[d] Pharmaceutical Chemistry Division, School of Advance Science, Vellore Institute of Technology University, Vellore 632014, Tamilnadu, India

ARTICLE INFO

Article history:
Received 11 July 2013
Revised 10 January 2014
Accepted 13 January 2014
Available online 31 January 2014

Keywords:
Pyrazolo[3,4-*d*]pyrimidine
Adenosine receptor antagonist
Homology modeling
Molecular docking
Structure affinity relationship

ABSTRACT

In the present study, a molecular simplification approach was employed to design novel bicyclic pyrazolo[3,4-*d*]pyrimidine (PP) derivatives from tricyclic pyrazolo[4,3-*e*]-1,2,4-triazolo-[1,5-*c*]pyrimidines (PTP) as promising human A_3 adenosine receptor (hA_3AR) antagonists. All the target compounds were synthesized using novel and efficient synthetic schemes and the structure–activity relationship studies of these PPs were explored through the synthesis of a series of PTP analogues with various substituents. Substituents with different lipophilicity and steric hindrance (e.g., alkyl and aryl–alkyl) functions were introduced at N^2 position of the pyrazole ring, while acyl groups with different electronic properties were introduced at C^6 position of the bicyclic nucleus to probe both electronic and positional effects. Most of the synthesized derivatives of the PP series presented good affinity at the hA_3AR, as indicated by the low micromolar range of K_i values and among them, compound **63** with N^2 neopentyl substituents showed most potent hA_3AR affinity with K_i value of 0.9 μM and high selectivity (hA_1AR/hA_3AR = >111 & $hA_{2A}AR/hA_3AR$ = >111) towards other adenosine receptor subtypes. Interestingly, small isopropyl groups at N^2 position displayed high affinity at another receptor subtype ($hA_{2A}AR$, e.g., compound **55**, with K_i $hA_{2A}AR$ = 0.8 μM), while they were less favorable at the hA_3AR. Molecular docking analysis was also performed to predict the possible binding mode of target compounds inside the hA_3AR and $hA_{2A}AR$. Overall, PP derivatives represent promising starting points for new AR antagonists.

1. Introduction

Adenosine is an endogenous nucleoside that mediates a wide range of physiological responses through interaction with specific adenosine receptors (ARs), which are G protein-coupled receptors (GPCRs) comprising the characteristic seven transmembrane domains connected by three extracellular (EL) and three intracellular (IL) loops. There are four basic types of ARs that have been cloned and pharmacologically characterized, namely, A_1, A_{2A}, A_{2B} and A_3 ARs.[1,2] Each of these ARs is associated with its own distinct biochemical pathways. Typically, the activation of adenosine receptors (ARs) can induce inhibition (A_1 and A_3) or activation (A_{2A} and A_{2B}) of the adenylate cyclase. In addition, other signaling pathways involving phospholipases C and D, Ca^{2+} and mitogen-activated protein kinases (MAPK) have also been described. In particular, A_3 adenosine receptor (A_3AR) subtype is implicated in pathological conditions such as cardiac and cerebral ischemia, neurodegenerative diseases as well as chronic inflammatory diseases including rheumatoid arthritis and asthma.[3,4] Furthermore, A_3AR has been found to be over expressed in some tumor cell lines, such as HL60 and K562 human leukemia,[5] jurkat lymphoma,[6] U937 monocytic macro phagichuman cell line,[7] A375 human melanoma,[8] human glioblastoma,[9] and human prostatic cells,[10] thus rendering the A_3AR an intriguing therapeutic target. Moreover, A_3ARs are involved in the tumor growth and in the regulation of cell cycle and mediate both pro- and anti-apoptotic effects closely associated with the level of receptor activation. It has been suggested that the selective inhibition of A_3ARs might result beneficial in several human pathologies (i.e. glaucoma and asthma), but

* Corresponding authors. Tel.: +65 6516 1876; fax: +65 6779 1554.
E-mail address: phapg@nus.edu.sg (G. Pastorin).

http://dx.doi.org/10.1016/j.bmc.2014.01.018
0968-0896/

antagonists could be also useful as diagnostic tools in diseases where hA_3ARs are over-expressed (i.e. cancer) thus stimulating the search for new selective A_3AR antagonists.

In the past few years, there has been an intensive effort to develop different heterocyclic scaffolds as hA_3AR antagonists. These scaffolds include pyridine and dihydropyridine analogues,[11] flavonoid,[12] isoquinoline,[13] triazoloquinazolines,[14] triazolo[4,3-*d*]pyrimidine,[15] pyrazolo-[3,4-*c*]or-[4,3-*c*]quinolines,[16] 2-phenylpyrazolo[4,3-*d*]pyrimidine-7-one,[17] pyrazolo[3,4-*d*]pyrimidine,[18] pyrazolo[4,3-*e*]-1,2,4-triazolo-[1,5-*c*]pyrimidines[19] (Fig. 1). Recently, it was reported a new series of 2-amino/2-oxoquinazoline-4-carboxamido derivatives, resulting from an in silico molecular simplification approach of the 1,2,4-triazolo[4,3-*a*]-quinoxalin-1-one template, which was extensively investigated in the search for new A_3AR antagonists.[20] Concurrently, an analogous strategy, applied to the same tricyclic skeleton, was confirmed to be effective for the identification of structurally simplified A_3AR antagonists with the advantage of less complex synthetic routes.[21]

This study promoted the 2-phenylphthalazin-1(2*H*)-one ring system (compound **5** in Fig. 1) as a new versatile scaffold suitable for further molecular manipulation. Moreover, a recent structure–activity relationship (SAR) study on the 2-phenyl-pyrazolo[4,3-*d*]pyrimidine-7-one (compound **6** in Fig. 1) and some simplified structures were reported[17], and these simplified analogues showed potent activity in the nanomolar range with improved selectivity towards the hA_3AR as compared to the parent compound. Overall, these studies proved the significance of simplified structures, which can act as hA_3AR antagonists to the same extent as more complex structures.

On the other hand, our group has recently reported new potent pyrazolo-triazolo-pyrimidines (PTPs) centered on the replacement of the conventional furan ring at position C^2 with a 2-(*para* substituted) phenyl ring and various substituents at N^5 and N^8 positions.[22] These new modifications not only enhanced the pharmacological profile of the antagonists significantly, but they also improved selectivity against the other adenosine receptor subtypes. However, PTP derivatives, and also most of the tricyclic compounds, have a number of limitations such as poor aqueous solubility due to high molecular weight and a complex nature of the structure, which makes the synthetic preparation difficult and time consuming. Moreover, these problems may affect the drug-like properties of the analogues.[23,24] Taking these drawbacks into account, the synthesis of more simplified heterocyclic derivatives has been scouted.[17,20,21]

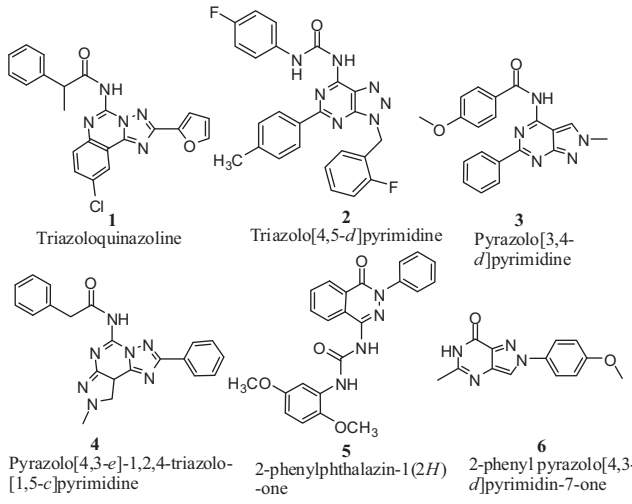

Figure 1. Examples of human A_3 adenosine receptor (hA_3AR) antagonists.

From the SAR studies of previously synthesized PTP derivatives,[22,25] we deduced certain features that could be vital for the hA_3AR antagonistic activity: (I) the pyrazolo[3,4-*d*]pyrimidine (PP) nucleus has shown to represent the core domain in the interaction with AR's binding sites, suggesting that its presence is critical in affecting the binding of this structure to the receptor of interest. Therefore, we proposed a new series of hA_3AR antagonists, in which the core PP domain was kept intact (Chart 1). (II) The size of the substituents at N^2 position of the PP bicyclic nucleus (corresponding to N^8 position of the PTP scaffold) could play an important role in determining the affinity and selectivity towards A_3 receptors. Our previous studies showed that small alkyl groups (e.g., methyl or ethyl) are well tolerated at the hA_3AR, since there is a steric control in the receptor pocket surrounding that position.[19] Hence, we introduced various substituents with different lipophilicity and steric hindrance such as alkyl (methyl **31**, isopropyl **32**, and neopentyl **33**) and phenyl ethyl (**34**) functions at N^2 position. III) Assuming that substituents at C^6 position (correspondent to position C^5 of PTP scaffold) are essential for retaining the selectivity and potency,[26] various acyl groups (benzoyl, *para* substituted benzoyl and phenyacetyl) were substituted at C^6 position in the new series of analogues. In fact, these moieties have given rise to potent hA_3AR antagonists when introduced at the C^5 position of the PTP scaffold.

Differently from the previous triazole ring in the PTP series, two types of substituents are introduced in our PP derivatives. First, a small steric chloro functional group at the C^4 position is chosen to allow the PP scaffold to hopefully attain the same binding pose as PTP due to restricted rotation of C^4 position while enabling a further point of functionalization. Second, a rotatable ethyl ester chain with hydrogen bonding property is introduced, in order to explore the effect of the different steric and rotatable bonds at the C^4 position. Thus, the development of a new class of compounds targeting the hA_3AR derives from a molecular simplification (Chart1) of the tricyclic PTP structure into a bicyclic pyrazolo[3,4-*d*]pyrimidine bearing key substituents, hoping that these new compounds could preserve their pharmacological profile at the hA_3AR while simplifying the synthetic procedures.

2. Results and discussion

2.1. Chemistry

The pyrazolo[3,4-*d*]pyrimidine derivatives **31–63** were prepared following four synthetic pathways, as depicted in Schemes 1–4.

Alkylation (or arylation) of 3-amino-4-pyrazole carbonitrile with alkyl (aryl) iodide or bromide in dry DMF, using dry potassium carbonate as a weak base, led to N^1 substituted regioisomer (**7–10**) as a major product. Among them, compounds **7** & **10** were already reported by our group.[22,27] In addition, compound **8** was also reported in the literature and was prepared by different procedure.[28]Subsequently,3-amino-N^1-substituted-4-pyrazolocarbonitriles (**7–10**) were hydrolyzed to corresponding carboxamides (**11–14**) under acidic conditions at cold temperature for 30 min, followed by stirring at ambient temperature for 5 h.

Among the carboxamide derivatives (**11–14**), compound **11** was already reported in the literature[29] and compound **12** was commercially available. Further, the carboxamide derivatives (**11–14**) were refluxed with benzoylisothiocyanate in acetone for 12 h, to be transformed into the benzoylthioureido derivatives (**15–18**). Treatment of **15–18** with a small excess of methyl iodide in aqueous sodium hydroxide solution at ambient temperature for 3 h gave the corresponding carbamidothioates **19–22**. The resulting methyl mercapto derivatives were heated in DMF containing 2% ammonia at 120 °C for 3 h in a sealed tube to afford benzoylguanidino

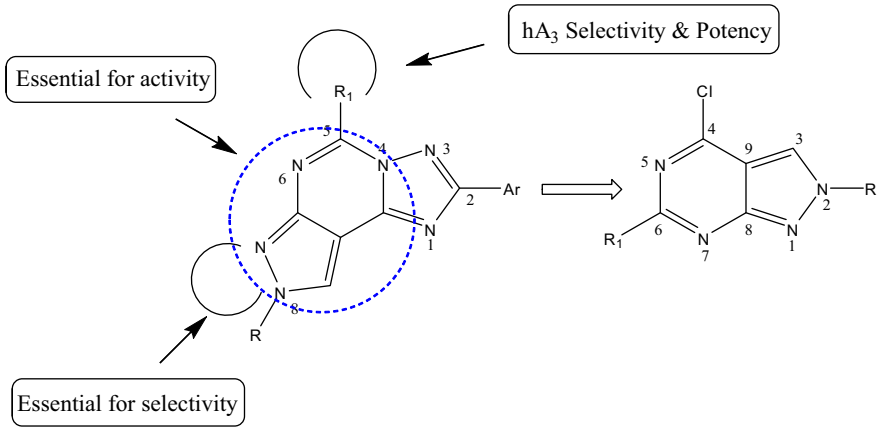

Chart 1. Rationale for the design of 2-(alkyl and arylalkyl substituted)-2*H*-pyrazolo [3,4-*d*]pyrimidine derivatives (molecular simplification of PTP into PP).

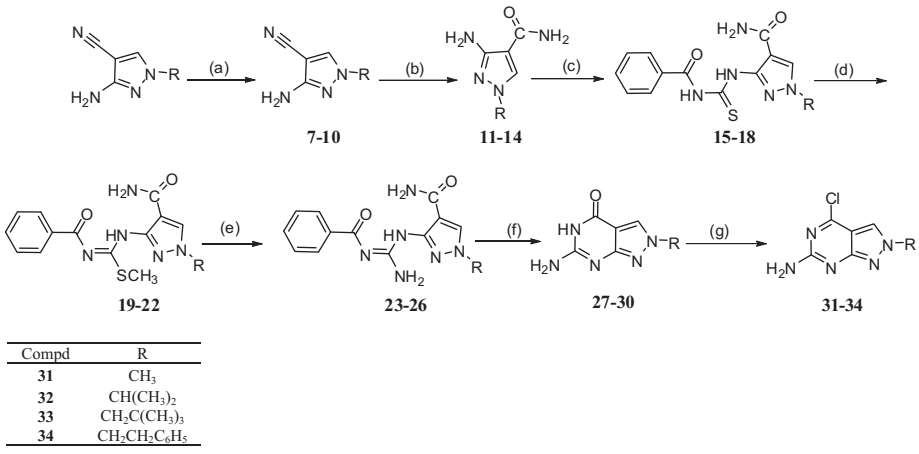

Compd	R
31	CH_3
32	$CH(CH_3)_2$
33	$CH_2C(CH_3)_3$
34	$CH_2CH_2C_6H_5$

Scheme 1. Reagents and conditions: (a) RI or RBr, K_2CO_3, DMF, 90 °C, 10 h; (b) conc H_2SO_4, 0 °C to rt, 5 h; (c) C_6H_5CONCS, acetone, reflux, 12 h; (d) CH_3I, 0.1 N NaOH, rt, 3 h; (e) 2% aq NH_3, DMF, 120 °C sealed tube, 3 h; (f) 1 N NaOH, reflux, 12 h; (g) $POCl_3$, dimethylaniline, reflux, 24 h.

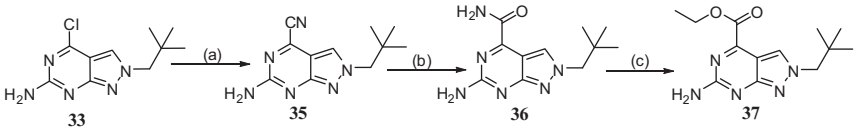

Scheme 2. Reagents and conditions: (a) NaCN, *p*-toluene sulfinate sodium, DMF, 80 °C, 2 h; (b) K_2CO_3, 30% H_2O_2, rt, 1 h; (c) EtOH, concd H_2SO_4, reflux, 12 h.

derivatives **23**–**26**. This nucleophilic substitution reaction was performed with slight modification from the previously reported procedure applied for the conversion of methyl carbamidothioates to guanidino derivatives.[30] Interestingly, the synthesized compounds **23**–**26** were insoluble in any of the solvent. Hence, they were directly taken to the next reaction. Hydrolysis of the benzoyl guanidine derivatives under basic conditions led to the corresponding free amines **27**–**30** with higher yields (from 68% to 81 %). In addition, compounds **27**–**30** are predominantly existed as tautomeric keto form. The predominant keto form was confirmed by the presence of amide protons (NH—C=O) signals between 10.4 and 10.6 ppm in the series using ^{1}H NMR spectroscopy. Conversely, the enol form of the tautomer (N=C—OH) containing OH proton was ruled out since it would have shown a signal at high down field of about 12 ppm in ^{1}H NMR spectroscopy. Subsequently, the 6-amino-2-alkyl-2*H*-pyrazolo[3,4-*d*]pyrimidin-4(5*H*)-ones (**27**–**30**) were further reacted with phosphoryl trichloride in the presence of dimethylaniline under reflux condition to form the corresponding chloro analogues (**31**–**34**). Among them, compound **31** was already reported by Seela et al. in low yield using different procedures.[31]

The structural determination of **31** in the solid state was carried out by using X-ray diffraction studies inorder to confirm the alkyl substitution at N^2 position. Single crystal of **31** was grown by vapor diffusion of diethyl ether into a saturated solution of MeOH. The detailed key crystallographic parameters can be found in the ESI (Table S1 & S2). The X-ray crystallographic results confirmed the successful substitution of the substituent (methyl group) at N^2 position (Fig. 2).

Compound **35** was prepared by treating **33** with sodium cyanide in the presence of *p*-toluene sulfinate sodium as catalyst in dry DMF at 80 °C for 2 h. The nitrile groups were detected by the presence of CN peak at 115 ppm at ^{13}C NMR. The resulting nitrile compound was hydrolysed through the 'Radziszewski reaction', using aqueous hydrogen peroxide and aqueous potassium carbonate in cold or hot condition.[32] However, the product was obtained with low yield in these conditions. Hence, with a slight

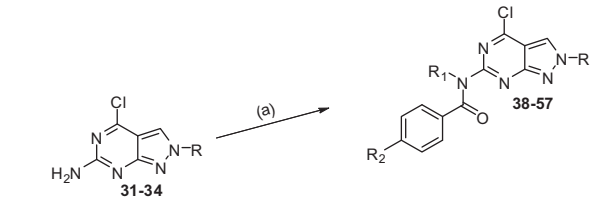

	R	R_1	R_2		R	R_1	R_2
31	CH_3	-	-	**48**	$CH_2C(CH_3)_3$	H	CF_3
32	$CH(CH_3)_2$	-	-	**49**	$CH_2C(CH_3)_3$	H	CH_3
33	$CH_2C(CH_3)_3$	-	-	**50**	$CH_2CH_2C_6H_5$	H	H
34	$CH_2CH_2C_6H_5$	-	-	**51**	$CH_2CH_2C_6H_5$	H	F
38	CH_3	H	H	**52**	$CH_2CH_2C_6H_5$	H	CF_3
39	CH_3	H	F	**53**	$CH_2CH_2C_6H_5$	H	CH_3
40	CH_3	H	CF_3	**54**	CH_3	C_6H_5CO	H
41	CH_3	H	CH_3	**55**	$CH(CH_3)_2$	C_6H_5CO	H
42	$CH(CH_3)_2$	H	H	**56**	$CH_2C(CH_3)_3$	C_6H_5CO	H
43	$CH(CH_3)_2$	H	F	**57**	$CH_2CH_2C_6H_5$	C_6H_5CO	H
44	$CH(CH_3)_2$	H	CF_3	**58**	CH_3	-	-
45	$CH(CH_3)_2$	H	CH_3	**59**	$CH(CH_3)_2$	-	-
46	$CH_2C(CH_3)_3$	H	H	**60**	$CH_2C(CH_3)_3$	-	-
47	$CH_2C(CH_3)_3$	H	F	**61**	$CH_2CH_2C_6H_5$	-	-

Scheme 3. Reagents and conditions: (a) substituted benzoyl chloride, DIPEA, toluene, reflux, 24 h; (b) phenyacetyl chloride, DIPEA, toluene, reflux, 24 h.

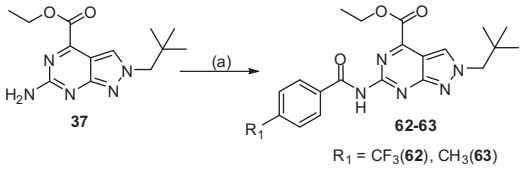

Scheme 4. Reagents and conditions: (a) substituted benzoyl chloride, DIPEA, toluene, reflux, 24 h.

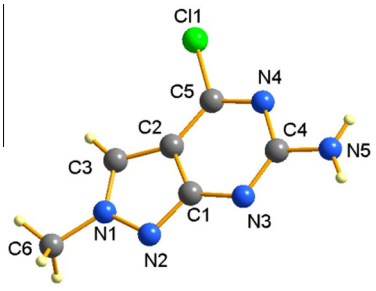

Figure 2. X-ray crystal structure of compound **31** (CCDC-937929). All the atoms are represented by spheres of arbitrary radii.

modification to the reported procedure, the reaction was carried out at a room temperature to obtain carbamide (**36**) with good yield. Subsequently, this intermediate compound (**36**) was esterified in the presence of concd H_2SO_4 with absolute ethanol under reflux condition to obtain the corresponding carboxylate **37** as solid.

Mono-and di-acylated derivatives of compounds **31**–**34** were synthesized by using substituted benzoyl chlorides or phenylacetyl chloride in different mole ratios (Scheme 2). Analogues **31**–**34** were treated with two equivalents of substituted benzoyl chloride and phenylacetyl chloride in the presence of diisopropylethylamine (DIPEA) to obtain the mono-benzoyl derivatives (**38**–**53**) and phenyl acetyl derivatives (**58**–**61**), respectively. Di-substituted benzoyl derivatives (**54**–**57**) of analogues **31**–**34** were prepared under this standard condition using 4 equiv of the benzoyl chloride and DIPEA.

Similarly, acylation of compound **37** was carried out as reported in Scheme 4. With a slight modification to the previous 4-chloro substituted pyrazolopyrimidines (**31**–**34**), 3 equiv of substituted benzoyl chlorides and diisopropylethylamine were used to obtain monoacylated compounds **62**–**63**.

2.2. Binding affinity and Structure–activity relationships

In this manuscript, we proposed to modify our previously synthesized tricyclic pyrazolo[4,3-*e*]-1,2,4-triazolo-[1,5-*c*]-pyrimidines (PTPs)[22] into a bicyclic pyrazolo[3,4-*d*]pyrimidine (PP) scaffold by considering the significance of simplified structures[17,20,21] that can act as promising antagonists, hopefully with similar or even improved affinity and selectivity at the hA_3AR. Towards that purpose, a new series of 2-(ar)alkyl-2*H*-pyrazolo[3,4-*d*]pyrimidines was successfully synthesized and characterized. The receptor binding affinities of the synthesized PTP simplified analogues (**31**–**34** & **37**) and their derivatives (**38**–**61** & **62**–**63**) are summarized in Table 1.

The binding affinity of antagonist was evaluated by measuring the displacement of selective radioligands which were previously bound to the receptor expressed (Chinese hamster ovary cells (CHO) for hA_1AR, $hA_{2A}AR$ and hA_3AR) at the cellular surface. In this assay, the displacement of (i) specific [^{3}H]CCPA binding at hA_1AR, (ii) specific [^{3}H]NECA binding at the $hA_{2A}AR$ and (iii) [^{3}H]HEMADO at the hA_3AR were evaluated. Due to the lack of a suitable radioligand for $hA_{2B}AR$, the antagonists activity was determined in adenylyl cyclase experiments in CHO cells expressing the $hA_{2B}AR$.[33,34] K_i (dissociation constant) value of the data was calculated using Cheng and Prusoff equation,[35] with geometric means of at least three experiments including 95% confidence intervals.

The binding assay results indicated that the reported molecular simplification of the PTP structure, although with a remarkable

Table 1
Binding affinity (K_i) of synthesized compounds at hA_1AR, $hA_{2A}AR$, and hA_3AR[a] and selectivity against hA_1AR and $hA_{2A}AR$ (R denotes N position, R_1 denotes C position)

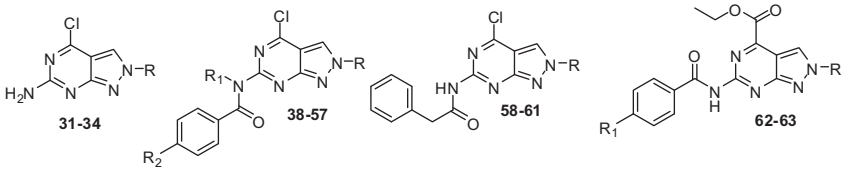

Compd	R	R_1	R_2	K_i, μM (95% CI)				Selectivity	
				hA_1[b]	hA_{2A}[c]	hA_{2B}[d]	hA_3[e]	hA_1/A_3	hA_{2A}/A_3
31	CH_3	—	—	29.7 (28.6–30.7)	9.1 (4.4–19.1)	>20	>100	>0.29	>0.09
32	$CH(CH_3)_2$	—	—	9.0 (6.4–12.5)	3.3 (1.5–7.2)	>10	>100	>0.09	0.03
33	$CH_2C(CH_3)_3$	—	—	12.0 (10.6–13.7)	4.1 (2.2–7.6)	>10	>60	>0.2	>0.6
34	$CH_2CH_2C_6H_5$	—	—	4.3 (2.9–6.4)	3.7 (3.4–4.1)	>20	>100	>0.04	>0.03
38	CH_3	H	H	>100	24.2 (7.7–76.5)	>20	23.6 (15.8–35.4)	>4.2	1.0
39	CH_3	H	F	>100	20.5 (12.7–33.2)	>20	31.9 (25.7–39.6)	>3.1	0.6
40	CH_3	H	CF_3	>100	25.6 (16–41)	>20	33.5 (28.2–39.7)	>2.9	0.7
41	CH_3	H	CH_3	.>100	12.0 (6.6–21.8)	>20	13.5 (5.8–31.2)	7.4	0.8
42	$CH(CH_3)_2$	H	H	19.6 (19.3–20)	4.6 (1.8–11.8)	>20	12.8 (6.9–23)	1.5	0.3
43	$CH(CH_3)_2$	H	F	3.4 (3.41–3.47)	1.6 (0.85–3.29)	>20	>60	>0.05	>0.02
44	$CH(CH_3)_2$	H	CF_3	13.8 (9.3–20.3)	2.7 (1.8–4.1)	>20	10.3 (6.0–17.6)	1.3	0.2
45	$CH(CH_3)_2$	H	CH_3	4.1 (2.3–7.4)	1.1 (0.66–2.0)	>20	>100	>0.04	0.01
46	$CH_2C(CH_3)_3$	H	H	11.0 (5.7–20.0)	3.5 (2.9–4.3)	⩾10	30.3 (17.4–52.7)	0.3	0.1
47	$CH_2C(CH_3)_3$	H	F	16.5 (6.8–39.8)	2.2 (1.6–3.1)	>10	5.9 (3.0–11.4)	2.7	0.3
48	$CH_2C(CH_3)_3$	H	CF_3	>100	>100	>20	6.6 (3.6–12.1)	>15	>15
49	$CH_2C(CH_3)_3$	H	CH_3	11.1 (7.3–16.6)	2.1 (1.8–2.4)	>10	5.0 (4.6–5.4)	2.2	0.4
50	$CH_2CH_2C_6H_5$	H	H	3.8 (2.2–6.5)	3.1 (2.3–4.3)	>20	8.6 (3.3–21.9)	0.4	0.3
51	$CH_2CH_2C_6H_5$	H	F	2.7 (2.1–3.4)	2.06 (0.83–5.06)	>20	>100	0.02	0.02
52	$CH_2CH_2C_6H_5$	H	CF_3	>60	16.4 (8.3–32.6)	>20	2.8 (1.7–4.5)	>21.4	5.8
53	$CH_2CH_2C_6H_5$	H	CH_3	10.8 (9.5–12.1)	9.9 (9.3–15.5)	>20	1.5 (0.71–3.2)	7.2	6.6
54	CH_3	C_6H_5CO	H	>60	17.5 (10.5–29.4)	>20	7.1 (6.2–8.1)	8.4	2.4
55	$CH(CH_3)_2$	C_6H_5CO	H	7.9 (7.6–8.1)	0.8 (0.61–1.2)	>20	6.7 (2.2–20.5)	1.1	0.1
56	$CH_2C(CH_3)_3$	C_6H_5CO	H	>100	~100	>20	6.5 (3.8–12.4)	>15.3	>15.3
57	$CH_2CH_2C_6H_5$	C_6H_5CO	H	>100	5.4	>20	2.9 (1.9–4.6)	>34.5	2
58	CH_3	—	—	16.3 (14–18.9)	29.9 (13–69.2)	>20	6.6 (2.6–16.9)	2.4	4.5
59	$CH(CH_3)_2$	—	—	1.9 (1.0–3.6)	4.7 (3.7–5.9)	>10	27.1 (18.5–39.7)	0.07	0.17
60	$CH_2C(CH_3)_3$	—	—	31.9 (26.4–38.6)	23.6 (9.5–58.2)	>20	10.9 (4.3–27.6)	2.9	2.1
61	$CH_2CH_2C_6H_5$	—	—	6.5 (3.9–10.7)	8.6 (5.0–14.9)	>20	11.4 (7.4–17.5)	0.5	0.7
62	$CH_2C(CH_3)_3$	CF_3	—	>100	>100	>20	1.3 (1.3–1.4)	>77	>77
63	$CH_2C(CH_3)_3$	CH_3	—	>100	>100	>20	0.9 (0.7–1.0)	>111	>111

[a] Adenylyl cyclase activity of synthesized compounds at the $hA_{2B}AR$.
[b] Displacement of specific [^{3}H]-CCPA binding at hA_1AR expressed in Chinese hamster ovary (CHO) cells (n = 3–6).
[c] Displacement of specific [^{3}H]-5′-*N*-ethylcarboxamido adenosine (NECA) binding at $hA_{2A}AR$ expressed in CHO cells (n = 3–6).
[d] K_i values for inhibition of NECA-stimulated adenylyl cyclase activity in CHO cells (n = 3–6).
[e] Displacement of specific [^{3}H]-2-(1-hexynyl)-N^6-methyl adenosine (HEMADO) binding at hA_3AR expressed in CHO cells (n = 3–6).

drop in the K_i values, still enabled the binding at the hARs (Table 1). This result seems very promising, considering that the PP represents a much smaller scaffold for the hA_3AR. Indeed, most of the pyrazolo[3,4-*d*]pyrimidines were able to maintain moderate affinity at hA_3 receptors as indicated by the low micromolar range (0.9–33.5 μM) of K_i values and a few compounds showed high selectivity towards the other receptor subtypes.

2.2.1. N^2 position

To examine the impact of the alkyl group substitutions at N^2-position on the pharmacological profile, we compared the binding assay results of the analogues bearing various alkyl substitutions (i.e. methyl, isopropyl and neopentyl) or a phenyl ethyl substitution at this position. First of all, all the synthesized compounds of this series are inactive towards the $hA_{2B}AR$ subtype. In fact, adenylate cyclase assays displayed K_i upper than 20 μM. The alkyl substitutents (methyl, isopropyl and neopentyl) at N^2 position of the pyrazole ring were found to modulate the affinity at hA_3AR to a considerable extent. Among them, N^2 isopropyl and N^2 methyl substituted analogues showed the lowest binding affinity towards hA_3AR (**38**–**45**, **54**, **55** & **59**) with K_i values between 10.3 and 33.5 μM, except for C^6-phenylacetamido compound **58** which displayed an affinity of 6.6 μM towards hA_3AR that is better than those of the other N^2-substituted analogues (**58** vs **59**–**61**). In addition, in the N^2 isopropyl series there are two inactive compounds at the hA_3AR (**43**, **45**) and, in general, they presented a better $hA_{2A}AR$ affinity profile (**42**–**45**, **55** and **59**, with K_i $hA_{2A}AR$ values between 0.8 and 4.7 μM).

Interestingly, neopentyl substituted analogues (**46**–**49** and **56**) of C^4-chloro series and C^4-carboxylate series exerted a relatively more favourable effect at the hA_3AR receptor. They also displayed a 3–5 fold increased affinity in comparison with the N^2 methyl derivatives, but only when a substituted phenyl group was present at the C^6 position (**47**–**49**). In fact, the presence of an unsubstituted phenyl moiety in compounds **60** and **46** lead to a lower affinity at the hA_3AR in respect to N^2-methyl analogues **58** and **38** (i.e. **60**, K_i hA_3AR = 10.9 μM vs **58**, K_i hA_3AR = 6.6 μM). Among all the C^4-chloro N^2 alkyl substituted derivatives (**38**–**49**, **54**–**56** & **58**–**60**), compound **49** showed the best affinity at the hA_3AR (K_i hA_3AR = 5 μM). Moreover, derivatives **48** (K_i hA_3AR = 6.6 μM) & **56** (K_i hA_3AR = 6.5 μM) of the same series are comparable to compound **49** in terms of affinity at the hA_3AR but exhibited the highest selectivity towards other receptor subtypes (**48** & **56**; hA_1AR/hA_3AR >15; $hA_{2A}AR$/hA_3AR >15). Similarly, few compounds with C^4 carboxylate group and N^2 neopentyl substitution showed higher affinity and selectivity as compared to the C^4 chloro counterparts.

Among them, compounds **62** & **63** displayed 4–6 fold improvement in affinity and 5–55 fold improvement in selectivity.

Finally, in C^4 chloro series the presence of a phenyl ethyl group at N^2 position generally resulted in a significant increase of hA_3 affinity (**50**–**53**, **57** and **61**, K_i hA_3AR values between 1.5 and 11.4 μM) and better selectivity in comparison to the other N^2 alkyl counterparts (**38**–**49** and **54**–**56** & **58**–**60**), except for compound **60**, which was unexpectedly inactive at the hA_3AR (K_i hA_3AR >100 μM). This result indicates that the phenylethyl group at N^2 position played a more essential role in the binding at the hA_3AR in C^4chloro series; in fact, it suggests that the steric hindrance far from N^2 position is more favourable for the bulky phenyl ethyl group to orient itself inside the binding cavity, in comparison with little groups in close proximity of N^2 position (i.e. **52** vs **44**). However, these findings are in contrast with the PTP scaffold, where small substituents (e.g., CH_3) at N^8 position are preferable than larger alkyl and aryl substituents.[19]

2.2.2. C^6 position

Analogues bearing a free amino group at C^6 (**31**–**34**) showed affinity towards the $hA_{2A}AR$ (K_i $hA_{2A}AR$ = 3.3–9.1 μM) and the hA_1-AR (K_i hA_1AR = 4.3–29.7 μM) subtypes but not towards the hA_3AR. This was somehow expected, as it was already observed that PTPs with a free amino group at C^5 position are able to bind hA_1AR and $hA_{2A}ARs$ better than hA_3ARs.

In addition, analogue **54**, bearing a dibenzoyl group at C^6 position, displayed an enhancement of affinity at the hA_3AR subtype (K_i hA_3AR = 7.1 μM) in comparison with the mono-acylated analogue (**38**, with K_i hA_3AR = 23.6 μM). When the C^6 group was replaced by a slightly longer phenyl acetyl group, affinity was maintained (**58**, with K_i hA_3AR = 6.6 μM) and selectivity versus the $hA_{2A}AR$ was increased (**54**, hA_1AR/hA_3AR = 2.4 vs **58**, hA_1AR/hA_3AR = 4.5). This indicates that the binding cavity is spacious enough to accommodate the bulky diacyl group and longer phenylacetyl group at C^6 position. In contrast, shorter chains like single benzoyl groups seemed less favourable.

As seen in Table 1, C^6 acyl substituents of N^2-isopropyl derivatives (**42**–**45**, **55** and **59**) impelled the affinity towards the $hA_{2A}AR$; in fact the best result was observed for the di-acylated analogue (**55**, with K_i $hA_{2A}AR$ = 0.8 μM). This derivative was also about 8–10 times more selective towards the hA_1AR and hA_3AR receptor subtypes. Also, the presence of additional functional groups at the *para* position of the C^6-benzoyl substituent maintained the affinity and remarkably increased the selectivity against the hA_3AR subtype, independently of the electronic nature of substituent. In fact, this behaviour was observed both for the electron donating methyl group (**45**, K_i $hA_{2A}AR$ = 1.1 μM, $hA_3AR/hA_{2A}AR$ = 91) and for the electron withdrawing group fluorine (**43**, with K_i $hA_{2A}AR$ = 1.6 μM, and $hA_3AR/hA_{2A}AR$ >37). Moreover, it was noted that high affinity towards the hA_{2A} subtype was reflected in the whole N^2 isopropyl series.

Nevertheless, affinity switched towards hA_3AR for the neopentyl series. Although the free amino group of neopentyl prompted a better affinity at the $hA_{2A}AR$ (**33**, K_i $hA_{2A}AR$ = 4.1 μM and K_i hA_3-AR >60 μM), corresponding acyl substitutions made a significant improvement in the affinity at hA_3ARs (e.g., **46**, K_i $hA_{2A}AR$ = 3.5 μM and K_i hA_3AR = 30 μM). Notably, replacement of C^6 benzoyl with groups in *para* (e.g., F, CF_3) slightly ameliorated the affinity towards the hA_3AR (e.g., **47**, with K_i hA_3AR = 5.9 μM & **48**, with K_i hA_3-AR = 6.6 μM**)**. Remarkably, while compound **49** (with an electron donating *para*-toluoyl group) and **47** (with an electron withdrawing *para*-F group) showed the best affinity at the hA_3AR (**49**, K_i hA_3-AR = 5.0 μM; **47**, K_i hA_3AR = 5.9 μM) in the neopentyl series, its *para*-CF_3 analogue **48** displayed the highest selectivity (hA_1AR/hA_3-AR >15, $hA_{2A}AR/hA_3AR$ >15) in the whole series. This indicates the different contributions of electron donating and electron withdrawing groups at the *para* position of the benzoyl group at C^6.

In the N^2-phenylethyl series, *para* unsubstituted benzoyl (**50**, with K_i hA_3AR = 8.6 μM) and chain lengthened phenylacetyl (**61**, with K_i hA_3AR = 11.4 μM) at the C^6 position, appeared to reduce moderately the affinity of the PP scaffold at the hA_3AR in comparison with the *para* substituted benzoyl derivatives (**52** & **53**). Similarly, *para*-F group (**51**, with K_i hA_3AR >−100 μM) in the acyl chain had a detrimental effect on hA_3AR, however, it showed good affinity towards hA_{2A} receptor subtype (K_i $hA_{2A}AR$ = 2.06 μM, $hA_3AR/hA_{2A}AR$ >50). On the other hand, analogue **53**, with the electron donating *para*-toluoyl substituent at C^6 position, displayed substantial increase in the affinity towards the hA_3 receptor (K_i hA_3-AR = 1.5 μM) and it also imparted a 6–8 fold increment in affinity in comparison with corresponding unsubstituted (**50**, K_i hA_3-AR = 8.6 μM and **61**, K_i hA_3AR = 11.4 μM) and neopentyl (**49**, K_i hA_3-AR = 5.0 μM) compounds, respectively. Similarly, analogue **52**, with an electron withdrawing *para*-CF_3 benzoyl group, also exhibited comparable affinity at the hA_3AR (K_i hA_3AR = 2.8 μM). Interestingly, a >36 fold increase in affinity was observed for the derivative with *para*-CF_3 substituent in comparison with the *para*-F analogue, overall indicating that bulky, either electron-donating or electron-acceptor functional groups, are preferred over less bulky groups for a better affinity at the hA_3AR.

In addition, a few compounds of the C^4 carboxylate series with C^6-benzamide substitution and N^2 neopentyl groups overall displayed the best affinity (K_i hA_3AR = 0.9 μM) and a remarkable improvement in selectivity towards other AR subtypes as compared to the C^4-chloro series. Also, when the *para* position of the C^4 carboxylates was substituted with the electron withdrawing steric CF_3 group, the activity and selectivity were increased by 5 fold (**62**, K_i hA_3AR = 1.3 μM, hA_1AR/hA_3AR = >77 & $hA_{2A}AR/hA_3$-AR = >77) as compared to its chloro counterpart (**48**). Similarly, when electron donating $-CH_3$ group was introduced at the *para* position of the benzamide chain, the affinity was further improved (**63**, K_i hA_3AR = 0.9 μM, hA_1AR/hA_3AR = >111 & $hA_{2A}AR/hA_3$-AR = >111) up to 5 fold and the selectivity was improved up to 50 fold towards hA_1AR & 278 fold towards $hA_{2A}AR$ as compared to the corresponding chloro compound (**49**). Moreover, this compound (**63**) showed the best pharmacological profile in the whole series. These changes are observed due to the additional carboxylate substitution at C^4 position. This strongly suggests that C^4 ester substituents, along with either electron withdrawing CF_3 or electron donating CH_3 groups in the *para* position of acyl chain, are highly essential for enhancing the affinity at hA_3AR and selectivity towards the other receptor subtypes. Molecular modeling studies further rationalized the reason for such an improvement.

In summary, structure–affinity relationship analysis showed that substituents at N^2, C^4 and C^6 positions play a key role in modulating the binding affinity and selectivity at the adenosine receptors. Our results confirmed the importance of the contemporary introduction in the PP system of (a) large lipophilic substituents (e.g., neopentyl and phenyethyl) at N^2 position to maintain the affinity at hA_3AR; (b) sterically bulky electron donating or electron withdrawing *para* substituted acyl chains at C^6 position to increase the affinity towards hA_3AR; (c) a slightly smaller chain (i.e. isopropyl) at N^2 to confer the affinity towards the $hA_{2A}AR$, if further study is intended on hA_{2A} receptor; (d) an ester substituent at C^4 position to increase the selectivity towards other receptor subtypes.

Among the newly synthesized PP derivatives, analogue **63**, with a neopentyl substitution at N^2 position and a *para*-methylbenzamide at C^6 position, possessed the best hA_3AR affinity profile (K_i hA_3AR = 0.9 μM) and >100 fold selectivity towards the hA_1 and $hA_{2A}ARs$. Overall, compounds of the C^4 chloro series showed weaker affinity and poorer selectivity as compared to C^4 ester

substituents. This difference was purely attributable to the additional ester substituents at C^4.

2.3. Molecular modeling studies

2.3.1. Homology modeling

The crystallographic structure of $hA_{2A}AR$ complexed with ZM-241385 as high affinity antagonist (PDB code: 3EML),[36] was used to build up homology model of the hA_3AR (Fig. S1). Although several $hA_{2A}AR$ crystal structures are available, considering the high resolution (2.6 A°) and accuracy of the structure, 3EML was selected as a template. Moreover, the accuracy of 3EML has been thoroughly investigated by various research groups,[17,22] thus substantiating our approach. The homology modelling was performed using programme Modeller 9.11[37–40] and the quality of the model was evaluated using the Ramachandran Plot. Subsequently, the prediction ability of the constructed hA_3AR homology model was evaluated in the molecular docking experiments using MOE programme.

2.3.2. Molecular docking

A molecular docking study was performed for the new 4-chloro-pyrazolo[3,4-*d*]pyrimidine (**31**–**34** and **38**–**61**)and pyrazolo[3,4-*d*]pyrimidine 4-carboxylate (**62**–**63)** derivatives on both hA_3AR and $hA_{2A}AR$ to identify the hypothetical binding mode at the hA_3AR and to rationalize the results obtained from the pharmacological evaluation. As reported in the experimental section, MOE was used as a docking programme for the pose inspection of the novel pyrazolo[3,4-*d*]pyrimidine derivatives in both $hA_{2A}AR$ and hA_3AR. All the newly synthesized pyrazolo[3,4-*d*]pyrimidine derivatives were docked into the orthosteric *trans*-membrane (TM) binding cavities of both adenosine receptors.

From the docking simulation analysis, most of the newly synthesized derivatives were seen to share a similar binding pose in the TM region of the hA_3AR. For these compounds, ligand-recognition occurred in the upper region of the TM bundle, and the pyrazolo[3,4-*d*]pyrimidine scaffold was surrounded by TMs 3, 5, 6, 7 with the acyl ring at the C^6 position located towards the intracellular environment. Figure 3 (panel A) presents the hypothetical binding pose of compound **53** at the hA_3AR, which possesses the highest hA_3AR affinity among all the newly synthesized derivatives (K_i hA_3AR = 1.5 μM). It appeared that the bicyclic pyrazolo[3,4-*d*]pyrimidine core was anchored within the binding cleft through an aromatic π–π stacking interaction with Phe168 (EL2). Moreover, the carbonyl group of the exocyclic acyl chain at the bicyclic core interacted with polar residue Asn250 (6.55), forming a lone stabilizing H-bonding interaction. In addition, the phenyl ring of the acyl chain was located deep within the ligand binding cavity and formed hydrophobic interactions with the highly conserved Trp243 (6.48), an important residue in receptor activation and antagonist binding. The N^2 phenyl ethyl chain of the ligand was directed towards the TM2 and TM3. Compound **53** also formed hydrophobic interaction with many residues in the binding cleft including Thr87(3.29), Leu90(3.33), Leu91(3.34), Val169(EL2), Met177(5.38), Trp243(6.48), Leu246(6.51), Tyr265(7.36), Leu264(EL3) and Ile268(7.39).

In contrast, the binding pattern of compounds bearing non bulky substituents, such as N^2-methyl and N^2-isopropyl derivatives, displayed slightly different binding pose as compared to **53**. The pyrazole ring of these compounds is directed towards the

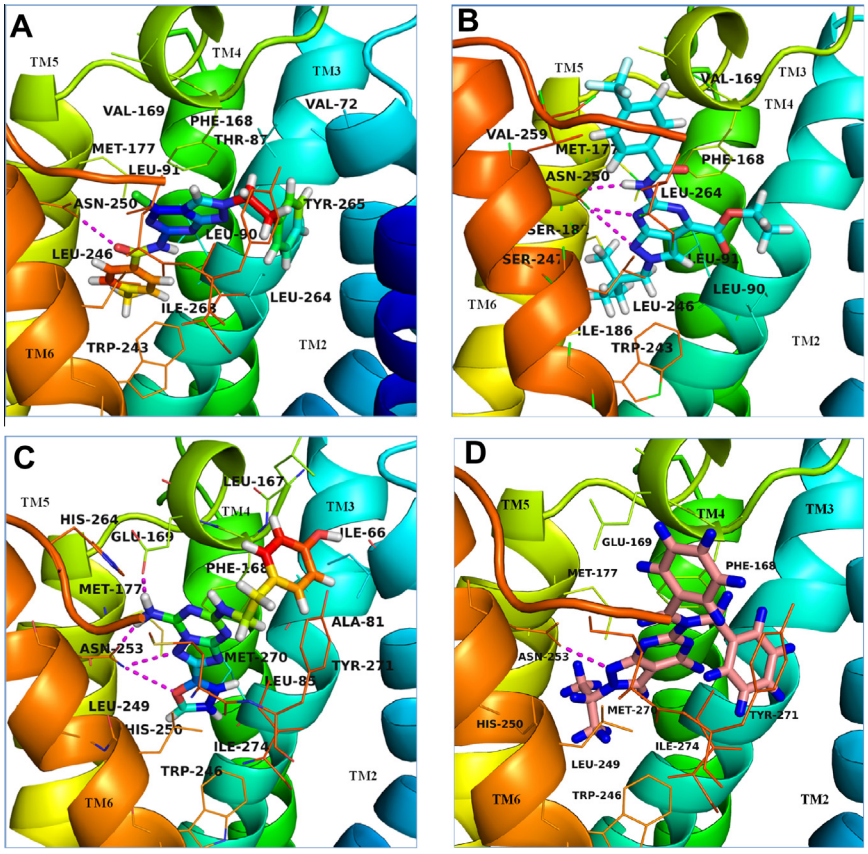

Figure 3. (A) Hypothetical binding mode of compound **53** obtained after docking simulations inside the hA_3AR binding site. (B) Hypothetical binding mode of compound **63** inside the hA_3AR binding site. (C) Crystallographic binding mode of ZM-241385 inside the $hA_{2A}AR$(PDB code 3EML) and (D) hypothetical binding mode of compound **55** inside the $hA_{2A}AR$ binding site and poses are viewed from the membrane side facing TM6, TM7, and TM1. The view of TM7 is omitted. Side chains of some amino acids important for ligand recognition and H-bonding interactions are highlighted. Hydrogen atoms are not displayed.

extracellular environment rather than towards TM2 and TM3, and also the main nucleus pyrazolo[3,4-*d*]pyrimidine was rotated of about 45° compared to the binding pose of compound **53**. Because of this different orientation of the molecule inside the binding cleft, these derivatives (**38**–**45** and **59**) might have lost the H-bonding interaction with Asn250 (6.55).The lack of these important interactions resulting from different orientation seems to be responsible for the lower affinity, as well as derivatives with less bulky groups at N^2 showed lower hA_3AR affinities (data not shown). However, as an exception, compound **54** and **58** in the N^2 methyl series and compound **55** in the isopropyl series showed a similar pattern as compound **53**, which in turn was reflected in the high binding activity of these compounds. Interestingly, the pyrazolo[3,4-*d*]pyrimidine derivatives bearing a lipophilic moieties at N^2 position, such as phenyl ethyl and neopentyl derivatives, shared similar binding pattern which accounted for high binding affinity of the compounds in these series (**52**,**53** & **57**). In fact, for all these derivatives, the pyrazolo[3,4-*d*]pyrimidine scaffold is utterly aligned inside the TM region of hA_3AR with the exception of compound **60** in the neopentyl series and compound **61** in the phenyl ethyl series. In particular, the aromatic stacking interaction with Phe168 (EL2), a lone H-bonding interaction with Asn250 (6.55) and the hydrophobic interaction with Trp243 (6.48) are conserved among these derivatives. As seen in Table 1, compounds **52** and **53** of the N^2 phenylethyl series and compounds **47**, **48** and **49** of the N^2 neopentyl series showed close binding affinity values which are reflected in the overlapping binding pattern with one another inside the binding cleft. Notably, due to the flexible nature of the neopentyl and phenylethyl substituents, which possess lengthy and multiple rotatable bonds (2 for neopentyl and 3 for phenylethyl), enabled the scaffold to obtain a different conformation to fit into the binding cleft. Although, compounds **46**–**48** of neopentyl series showed comparable affinity towards hA_3AR, the selectivity against hA_1AR and $hA_{2A}AR$ was improved for compound **48**, because of the *para*-CF_3 group. As seen from the docking studies, at the $hA_{2A}AR$, the hydrophobic side cleft delimited by TM2 and TM3 could accommodate less steric *para*-substituted compounds [i.e. **47** (F) and **49** (CH_3)], but could hardly accommodate the slightly bulkier *para*-CF_3(**48**). This steric effect could be accounted for the difference in affinity of compound **48** at $hA_{2A}AR$ versus **47** and **49**. Therefore, it is deduced that the presence of sterically bulky but lengthy chains at N^2 position ensures high binding affinity of the derivatives at the hA_3AR.

Interestingly, C^4-carboxylate N^2 neopentyl substituted benzamide compounds (**62** and **63**) displayed a different binding pose in comparison to compound **53**. Among them, compound **63** (Fig. 3B), which was the most potent analogue of the C^4-carboxylate series, oriented a little away from the centre of the binding pocket, towards the TM5. In addition, the ester group was oriented towards the TM2 and the phenyl ring of the benzamide pointed towards the ECL2. Due to this reason, the additional ester group was able to make a potential hydrogen bonding interaction with Asn250. Surprisingly, three stabilizing hydrogen bonding interactions were observed between ligand **63** and Asn250. Among them, one of the hydrogen bonding was seen with NH of the amide chain, and other two bondings were observed with the N-1 of the pyrazole and N-2 of pyrimidine, respectively. Similarly, another potent and selective compound of the series, compound **62**, also shared with **63** a close resemblance of the binding pose and was also involved in similar binding interactions. This in turn reflected the higher binding affinity and selectivity of these compounds. In both compounds (**62** and **63**), *para*-CF_3 and *para*-CH_3 made identical hydrophobic interaction with residues such as Val169, Val259 and Leu264 and one of the residues, Val169, was also reported in previous work on PTP analogues, where Val169 was deemed to be essential for antagonist recognition.[22] In addition, the neopentyl chain enabled the hydrophobic interaction with Trp243, Leu91, Ser181 and Ser247. The central PP scaffold was involved with an essential π–π stacking interaction with Phe168, which is considered to be crucial for the hA_3 antagonistic activity.[22] Notably, this interaction was also present in the binding modes of 4-chloro PP and PTPs. Data from literature suggest the importance of the binding of the Phe168 and the mutagenesis analyses conducted at the $A_{2A}AR$ demonstrated the importance of Phe168 for antagonist binding.[22]

Among the isopropyl derivatives, compound **55** (Fig. 3 panel D), with diacyl substitution at C^6 position and with the highest $hA_{2A}AR$ affinity (K_i = 0.8 μM) among all the isopropyl derivatives, showed a binding pattern close to ZM-241385. Notably, impeded free rotation of isopropyl group due to ring constraints directed the ligand to obtain a fixed conformation and this accounted for the shifting of affinity towards the $hA_{2A}AR$. The isopropyl substituents of the main scaffold are located towards the TM2, one of the diacyl chains pointing towards the EL2, whereas other acyl chains pointed towards the TM6. This result indicates that the receptor pocket, where the C^6 appended moiety of these derivatives accommodated is roomy enough to hold the rather bulky and broadened diacyl chain. In addition, N^1 of the pyrazole ring formed a H-bonding interaction with Asn253 (6.55) and a stable interaction with Glu169 (EL2), which is considered to be vital for ligand binding at the $hA_{2A}AR$.[41–43] Similarly, compound **45**, with a *para*-toluoyl group of the C^6-benzoyl substituent, bound to $hA_{2A}AR$ in a similar fashion as compound **55**, thus justifying an equally potent affinity at this receptor subtype. The electrostatic contribution per residue to the whole interaction energy for the ZM-241385 in $hA_{2A}AR$ (Fig. S2-D) was compared to the one of compound **53** inside the $hA_{2A}AR$. It was noticed that the three main stabilizing residues such as Glu169 (EL2), Asn253 (6.55), and Tyr271 (7.36) contributed for the affinity of ZM-241385 in the $hA_{2A}AR$. In contrast, compound **53** displayed slightly different binding mode, which in turn reflected in weak stabilizing interaction with these three residues (Fig. S2-E).

Eventually, we compared the binding pose of the most potent compounds of both chloro (**53**) and ester series (**63**) inside the hA_3-AR. It was observed that compound **63** was oriented in a different pattern from compound **53** of the chloro series. It is speculated that rotatable ester chain at C^4 position caused the ligand to attain different conformation. However, compound **63** retained all essential hydrophobic interactions with residues such as Met177, Leu246, Leu264, Trp243, Val169 and Val259. As seen earlier, compound **63** gained an extra stabilizing hydrogen bonding interaction with Asn250, whereas with compound **53**, a single hydrogen bonding interaction was observed (Fig. 3A). These findings substantiate the experimental results of increased affinity and selectivity for compound **63** over compound **53**.

Docking evaluation confirmed why newly synthesized PP-4-carboxylate derivatives are better than the 4-chloro-PP derivatives. Apparently, compounds of the PP-4-carboxylate series made an additional stabilizing hydrogen bonding interaction with the Asn250, which was not found with previous PP-chloro series derivatives. In addition, the most potent compounds of the series displayed some specific hydrophobic interactions with Val169 and Val259. These hydrogen bonding and hydrophobic interactions have remarkably contributed to the improved affinity and selectivity.

3. Conclusions

In summary, the bicyclic pyrazolo[3,4-*d*]pyrimidine scaffold was designed based on the molecular simplification approach from the tricyclic pyrazolo-triazolo-pyrimidine. In addition, all the target compounds were synthesized using a novel and efficient synthetic approaches. This study has led to the identification of a

novel series of pyrazolo[3,4-*d*]pyrimidine derivatives as selective hA_3AR or $hA_{2A}AR$ antagonists. The present study has highlighted that the pyrazolo-pyrimidine moiety is a promising scaffold for obtaining novel human AR antagonists. Indeed, most of the synthesized compounds showed affinity at the hA_3AR in the low micromolar range, with the most potent antagonist bearing a C^4 carboxylate and N^2 neopentyl with a C^6 *para*-toluoyl group (**63**, K_i hA_3AR = 0.9 μM, hA_1AR/hA_3AR = >111 & $hA_{2A}AR/hA_3AR$ = >111) and its fluorinated acyl derivative (**62**, K_i hA_3AR = 1.3 μM, hA_1AR/hA_3AR = >77 & $hA_{2A}AR/hA_3AR$ = >77). In addition, most of the compounds of the N^2 isopropyl series exhibited affinity in very low micromolar range towards $hA_{2A}AR$, especially compound **55** (K_i $hA_{2A}AR$ = 0.8 μM), which displayed the most potent affinity at $hA_{2A}AR$, whereas compounds **45** and **43** displayed remarkable selectivity towards the hA_3AR subtype (**45**, $hA_3AR/hA_{2A}AR$ >91; **43**, $hA_3AR/hA_{2A}AR$ >38).

To delineate the SAR of this pyrazolo[3,4-*d*]pyrimidine series as hA_3AR and $hA_{2A}AR$ antagonists, we have investigated different portions of this structure, modifying the substituents at the C^6, N^2 and C^4 positions. It emerged that, within the pyrazolo[3,4-*d*]pyrimidine nucleus, certain functionalities such as C^4 carboxylate, the acyl linkage at C^6 position and chain-elongated lipophilic alkyl groups or phenylethyl groups at N^2 position are important for the activity of these compounds at the hA_3AR; conversely, an isopropyl group at N^2 position is essential for activity at $hA_{2A}AR$. Through a molecular modeling investigation, the experimental findings have been rationalized by depicting the hypothetical binding mode between these newly synthesized series and the specific amino acid residues within the binding site of hA_3AR and $hA_{2A}AR$. Generally, binding assay results exemplified that C^4 ester substituted derivatives (**62**–**63**) are more potent than that of C^4 chloro substituted compounds (**38**–**61**) due to additional stabilizing interactions at the receptor site. Although the simplified analogues showed lower affinity as compared to the parent PTP analogues, this could be considered as the starting point for developing more potent hA_3AR antagonists. Further synthetic and biological studies on these C^4 carboxylate series lead structures are on-going in our laboratories and will be reported in due course.

4. Experimental section

4.1. Chemistry

Reactions were routinely monitored by thin-layer chromatography (TLC) on silica gel plate (precoated 60 F_{254} Merck plate). Column chromatographies were performed using silica gel 60 (Merck,70–230 mesh). Melting points were determined on a Gallenkamp instrument and were uncorrected. Compounds were dissolved in HPLC (high performance liquid chromatography) grade methanol for determination of mass to charge *m*/*z* on a LCQ Finnigan MAT mass spectrometer (source of ionization: Electron spin ionization (ESI) probe). Purity of the compounds were determined by HPLC using HITACHI, *version* 3.1.8b. ^1H and ^{13}C NMR spectra were determined in the deuterated dimethylsulfoxide (DMSO-d_6) solutions on Bruker DPX ultrashield NMR (400 MHz) spectrometers, with chemical shifts given in parts per million (δ) downfield relative to tetramethylsilane (TMS) as internal standard, and *J* values (coupling constants) given in hertz. The following abbreviations were used: s, singlet; d, doublet; t, triplet; sep, septet; m, multiplet; br, broad.

4.2. General procedure for the synthesis of 3-amino-1-alkyl or arylalkyl-1*H*-pyrazole-4- carbonitriles (7–10)

To a solution of 3-amino-1*H*-pyrazole-4-carbonitrile (1.08 g, 0.01 mol) in anhydrous DMF (5 mL), anhydrous potassium carbonate (1.65 g, 0.012 mol, 1.2 equiv) was added at 0 °C and the resulting mixture was stirred at the same temperature for 45 min. Appropriate alkyl/aryl iodide or bromide (0.012 mol, 1.2 equiv) was added slowly over 15 min and the reaction mixture was heated at 90 °C for 10 h. Then the resulting reaction mixture was cooled, poured over ice cold water and the aqueous phase was extracted with EtOAc (3 × 10 mL), the combined organic layers were dried over Na_2SO_4, filtered, and the solvent was removed under reduced pressure to give a oily residue that was purified via column chromatography eluting with a mixture of hexane/ethylacetate (1:1) to obtain the desired products **(7–10)** as solids.

4.2.1. 3-Amino-1-methyl-1*H*-pyrazole-4-carbonitrile (7)

Pale yellow solid: Yield (0.723 g, 67%); mp 125–127 °C.

4.2.2. 3-Amino-1-isopropyl-1*H*-pyrazole-4-carbonitrile (8)

Pale yellow solid: Yield (0.745 g, 69%); mp 120–122 °C.

4.2.3. 3-Amino-1-neopentyl-1*H*-pyrazole-4-carbonitrile (9)

Pale yellow solid: Yield (0.766 g, 71%); mp 123–125 °C. ^1H NMR (400 MHz, DMSO-d_6): δ 0.88 (s, 9H, $3CH_3$), 3.67 (s, 2H, CH_2), 5.49 (s, 2H, NH_2), 8.04 (s, 1H, pyrazole-H). LC–MS (ESI) analysis (*m*/*z*) calcd for $C_9H_{14}N_4$ (178.23): found 179.2 $[M+H]^+$.

4.2.4. 3-Amino-1-phenethyl-1*H*-pyrazole-4-carbonitrile (10)

Pale yellow solid: Yield (0.820 g, 76%); mp 132–134 °C.

4.3. General procedure for synthesis of 3-amino-1-(alkyl or aryl alkyl)-1*H*-pyrazole-4-carboxamide (11–14)

Carbonitriles **7**–**10** (0.03 mol) was dissolved in 7 mL concd H_2SO_4 at 0 °C and stirred at room temperature for 5 h. Then the reaction mixture was poured into ice cold water and neutralized to pH 7 with 28% NH_3 solution. The white precipitate was formed which was further washed with cold water and dried under vacuum.

4.3.1. 3-Amino-1-methyl-1*H*-pyrazole-4-carboxamide (11)

White solid: Yield (3.0 g, 83%); mp 155–157 °C.

4.3.2. 3-Amino-1-isopropyl-1*H*-pyrazole-4-carboxamide (12)

White solid: Yield (3.82 g, 85%); mp 159–161 °C.

4.3.3. 3-Amino-1-neopentyl-1*H*-pyrazole-4-carboxamide (13)

White solid: Yield (4.17 g, 78%); mp 161–163 °C. ^1H NMR (400 MHz, DMSO-d_6): δ 0.90 (s, 9H, $3CH_3$), 3.64 (s, 2H, CH_2), 5.32 (s, 2H, NH_2), 6.72 (br s, 1H, NH), 7.21 (br, 1H, NH), 7.85 (s, 1H, pyrazole-H). LC–MS (ESI) analysis (*m*/*z*) calcd for $C_9H_{16}N_4O$ (196.25): found 197.1 $[M+H]^+$.

4.3.4. 3-Amino-1-phenethyl-1*H*-pyrazole-4-carboxamide (14)

White solid: Yield (5.73 g, 90%); mp 166–168 °C. ^1H NMR (400 MHz, DMSO-d_6): δ 3.08 (t, J = 7.16 Hz, 2H, CH_2), 4.12 (t, J = 7.16 Hz, 2H, CH_2), 5.44 (s, 2H, NH_2), 6.24 (br s, 1H, NH), 6.74 (br s, 1H, NH), 7.19–7.35 (m, 5H, Ar-H), 7.80 (s, 1H, pyrazole-H). LC–MS (ESI) analysis (*m*/*z*) calcd for $C_{12}H_{14}N_4O$ (230.27): found 231.0 $[M+H]^+$, 254.2 $[M+Na]^+$.

4.4. General procedure for synthesis of 3-(3-benzoylthioureido)-1-(alkyl or aryl alkyl)-1*H*-pyrazole-4-carboxamide (15–18)

To a solution of carboxamides **11**–**14** (0.015 mol) in dry acetone (10 mL), benzoyl isothiocyante (0.0165 mol, 1.1 equiv) was added and refluxed at 60 °C for 12 h. The reaction mixture was cooled. The resulting yellow solid was filtered, washed with acetone and

dried under vacuum. The crude product was further recrystalized from methanol to obtain a pure solids.

4.4.1. 3-(3-Benzoylthioureido)-1-methyl-1*H*-pyrazole-4-carboxamide (15)

Yellow solid: Yield (1.28 g, 61%); mp 218–220 °C. ^{1}H NMR (400 MHz, DMSO-d_6): δ 3.61 (s, 3H, N–CH_3), 7.17 (br s, 1H, NH), 7.46–7.60 (m, 5H, CH), 7.73 (d, 2H, $CONH_2$), 7.78 (s, 1H, pyrazole-H), 11.47 (br s, 1H, NH). LC–MS (ESI) analysis (*m*/*z*) calcd for $C_{13}H_{13}N_5O_2S$ (303.34): found 304.0 $[M+H]^+$.

4.4.2. 3-(3-Benzoylthioureido)-1-isopropyl-1*H*-pyrazole-4-carboxamide (16)

Yellow solid: Yield (1.58 g, 63%); mp 212–214 °C. ^{1}H NMR (400 MHz, DMSO-d_6): 1.42 (d, J = 5.76 Hz, 6H, $2CH_3$), 4.44–4.50 (m, 1H, CH), 7.07 (br, 1H, NH), 7.57–7.68 (m, 5H, CH), 8.00 (d, 2H, $CONH_2$), 8.31 (s, 1H, pyrazole-H), 11.06 (br s, 1H, NH). LC–MS (ESI) analysis (*m*/*z*) calcd for $C_{15}H_{17}N_5O_2S$ (331.39): found 332.0 $[M+H]^+$.

4.4.3. 3-(3-Benzoylthioureido)-1-neopentyl-1*H*-pyrazole-4-carboxamide (17)

Yellow solid: Yield (1.76 g, 60%); mp 215–217 °C. ^{1}H NMR (400 MHz, DMSO-d_6): δ 0.91 (s, 9H, $3CH_3$), 3.91 (s, 2H, CH_2), 7.09 (br s, 1H, NHCO), 7.57–7.70 (m, 5H, CH), 8.00 (d, 2H, $CONH_2$), 8.18 (br s, 1H, pyrazole-H). LC–MS (ESI) analysis (*m*/*z*) calcd for $C_{17}H_{21}N_5O_2S$ (359.45): found 360.2 $[M+H]^+$.

4.4.4. 3-(3-Benzoylthioureido)-1-phenethyl-1*H*-pyrazole-4-carboxamide (18)

Yellow solid: Yield (2.44 g, 71%); mp 208–210 °C. ^{1}H NMR (400 MHz, DMSO-d_6): δ 3.07 (br d, 2H, CH_2), 4.34 (brs, 2H, CH_2), 7.21–7.27 (m, 5H, CH), 7.49–7.69 (m, 5H, CH), 7.99 (s, 2H, $CONH_2$), 8.01 (s, 1H, pyrazole-H), 11.51 (br s, 1H, NHCO), 12.7 (br s, 1H, NH). LC–MS (ESI) analysis (*m*/*z*) calcd for $C_{20}H_{19}N_5O_2S$ (393.46): found 393.9 $[M+H]^+$.

4.5. General procedure for synthesis of (*E*)-methyl *N*′-benzoyl-*N*-(4-carbamoyl-1-(alkyl or aryl alkyl)-1*H*-pyrazol-3-yl) carbamimidothioate (19–22)

To a solution of benzoylthioureidos **15**–**18** (0.003 mol) in 10 mL of 0.1 N NaOH, methyl iodide (0.0036 mol, 1.2 equiv) was added at room temperature and the resulting mixture was stirred for 3 h. The white suspension was observed and it was adjusted to pH 6 with glacial acetic acid. The white precipitate was obtained, which was filtered and washed with cold water and finally dried under vacuum.

4.5.1. (*E*)-Methyl-*N*′-benzoyl-*N*-(4-carbamoyl-1-methyl-1*H*-pyrazol-3-yl) carbamimidothioate (19)

White solid: Yield: (0.682 g, 75%); mp 196–198 °C. ^{1}H NMR (400 MHz, DMSO-d_6): δ 2.44 (s, 3H, SCH_3), 3.57 (s, 3H, N–CH_3), 7.00 (s, 1H, NH), 7.42–7.52 (m, 5H, CH), 7.70 (br s, 1H, pyrazole-H), 7.78 (d, 2H, $CONH_2$), 11.52 (br s, 1H, NH). LC–MS (ESI) analysis (*m*/*z*) calcd for $C_{14}H_{15}N_5O_2S$ (317.37): found 318.1 $[M+H]^+$.

4.5.2. (*E*)-Methyl-*N*′-benzoyl-*N*-(4-carbamoyl-1-isopropyl-1*H*-pyrazol-3-yl) carbamimidothioate (20)

White solid: Yield: (0.665 g, 67%); mp 223–225 °C. ^{1}H NMR (400 MHz, DMSO-d_6): 1.45 (d, J = 6.52 Hz, 6H, $2CH_3$), 2.41 (s, 3H, SCH_3), 4.59 (br s, 1H, CH), 7.39–7.91(m, 5H, CH), 8.02 (d, 2H, $CONH_2$), 8.24 (s, 1H, pyrazole-H), 13.09 (br s, 1H,NH). LCMS (ESI) analysis (*m*/*z*) calcd for $C_{16}H_{19}N_5O_2S$ (345.42): found 346.0 $[M+H]^+$.

4.5.3. (*E*)-Methyl-*N*′-benzoyl-*N*-(4-carbamoyl-1-neopentyl-1*H*-pyrazol-3-yl) carbamimidothioate (21)

White solid: Yield: (0.600 g, 56%); mp 219–221 °C. ^{1}H NMR (400 MHz, DMSO-d_6): δ 0.90 (s, 9H, $3CH_3$), 2.42 (s, 3H, SCH_3), 4.02 (s, 2H, CH_2), 7.40–7.95 (m, 5H, CH), 8.02 (d, 2H, $CONH_2$), 8.17 (s, 1H, pyrazole-H). LC–MS (ESI) analysis (*m*/*z*) calcd for $C_{18}H_{23}N_5O_2S$ (373.47): found 374.1 $[M+H]^+$, 396.2 $[M+Na]^+$.

4.5.4. (*E*)-Methyl-*N*′-benzoyl-*N*-(4-carbamoyl-1-phenethyl-1*H*-pyrazol-3-yl) carbamimidothioate (22)

White solid: Yield: (0.743 g, 63%); mp 235–237 °C. ^{1}H NMR (400 MHz, DMSO-d_6): δ 2.41 (s, 3H, SCH_3), 3.13 (t, J = 7.04 Hz, 2H, CH_2), 4.45 (t, J = 6.64 Hz, 2H, CH_2), 7.11–7.23 (m, 5H, CH), 7.39–7.87 (m, 5H, CH), 8.00 (d, 2H, $CONH_2$), 8.12 (s, 1H, pyrazole-H), 13.10 (br s, 1H, NH). LC–MS (ESI) analysis (*m*/*z*) calcd for $C_{21}H_{21}N_5O_2S$ (407.49): found 408.2 $[M+H]^+$, 430.2 $[M+Na]^+$.

4.6. General procedure for synthesis of (*Z*)-3-(2-benzoylguanidino)-1-(alkyl or aryl alkyl)-1*H*-pyrazole-4-carboxamide (23–26)

Carbamimidothioate derivatives **19**–**22** (0.003 mol) were dissolved in dry DMF (5 mL) containing 2% ammonia (5 mL) and heated to 120 °C for 3 h in a sealed tube. At the end of the reaction the odour of methyl mercaptan was recognized, cooled and poured over ice water mixture. The resulting white precipitate was washed with water and dried under vacuum.

4.6.1. (*Z*)-3-(2-Benzoylguanidino)-1-methyl-1*H*-pyrazole-4-carboxamide (23)

White solid: Yield (0.504 g, 53%); mp >300 °C. Insoluble.

4.6.2. (*Z*)-3-(2-Benzoylguanidino)-1-isopropyl-1*H*-pyrazole-4-carboxamide (24)

White solid: Yield (0.642 g, 62%); mp >300 °C. Insoluble.

4.6.3. (*Z*)-3-(2-Benzoylguanidino)-1-neopentyl-1*H*-pyrazole-4-carboxamide (25)

White solid: Yield (0.627 g, 56%); white mp >300 °C. Insoluble.

4.6.4. (*Z*)-3-(2-Benzoylguanidino)-1-phenethyl-1*H*-pyrazole-4-carboxamide (26)

White solid: Yield (0.646 g, 53%); mp >300 °C. Insoluble.

4.7. General procedure for synthesis of 6-amino-2-(alkyl or aryl alkyl)-2*H*-pyrazolo[3,4-*d*]pyrimidin-4(5*H*)-one (27–30)

A suspension of benzoylguanidino derivatives **23**–**26** (0.0035 mol) in 1 N NaOH (10 mL) was refluxed at 110 °C for 12 h. The resulting milky white mixture was adjusted to pH 6 with acetic acid. A mixture of benzoic acid and free amine derivatives were obtained which was washed with water and dried. Finely divided powder was suspended in hot ethanol with stirring to remove benzoic acid and filtered hot. The resulting ethanolic portion was evaporated to dryness to obtain a pure desired product as white solid.

4.7.1. 6-Amino-2-methyl-2*H*-pyrazolo[3,4-*d*]pyrimidin-4(5*H*)-one (27)

White solid: Yield (0.721 g, 72%); mp >300 °C. ^{1}H NMR (400 MHz, DMSO-d_6): δ 3.69 (s, 3H, N–CH_3), 6.69 (s, 2H, NH_2), 7.73 (s, 1H, pyrazole-H), 10.58 (s, 1H, NHCO). LC–MS (ESI) analysis (*m*/*z*) calcd for $C_6H_7N_5O$ (165.16): found 166.1 $[M+H]^+$.

4.7.2. 6-Amino-2-isopropyl-2*H*-pyrazolo[3,4-*d*]pyrimidin-4(5*H*)-one (28)

White solid: Yield (0.825 g, 75%); mp >300 °C. ^{1}H NMR (400 MHz, DMSO-d_6): δ 1.42 (d, J = 6.52 Hz, 6H, $2CH_3$), 4.50 (sep, J = 6.52 Hz, 1H, CH), 6.90 (s, 2H, NH_2), 8.11 (s, 1H, pyrazole-H), 10.61 (s, 1H, NHCO). LC–MS (ESI) analysis (*m*/*z*) calcd for $C_8H_{11}N_5O$ (193.21): found 194.2 $[M+H]^+$, 216.0 $[M+Na]^+$.

4.7.3. 6-Amino-2-neopentyl-2*H*-pyrazolo[3,4-*d*]pyrimidin-4(5*H*)-one (29)

White solid: Yield (0.815 g, 68%); mp >300 °C. ^{1}H NMR (400 MHz, DMSO-d_6): δ 0.96 (s, 9H, $3CH_3$), 3.70 (s, 2H, CH_2), 6.24 (s, 2H, NH_2), 7.67 (s, 1H, pyrazole-H). LC–MS (ESI) analysis (*m*/*z*) calcd for $C_{10}H_{15}N_5O$ (221.26): found 222.0 $[M+H]^+$, 244.0 $[M+Na]^+$

4.7.4. 6-Amino-2-phenethyl-2*H*-pyrazolo[3,4-*d*]pyrimidin-4(5*H*)-one (30)

White solid: Yield (1.067 g, 81%); mp >300 °C. ^{1}H NMR (400 MHz, DMSO-d_6): δ 3.10 (t, J = 6.64 Hz, 2H, CH_2), 4.36 (t, J = 6.76 Hz, 2H, CH_2), 7.34 (s, 2H, NH_2), 7.14–7.30 (m, 5H, CH), 7.89 (s, 1H, pyrazole-H), 10.62 (s, 1H, NHCO). LC–MS (ESI) analysis (*m*/*z*) calcd for $C_{13}H_{13}N_5O$ (255.28): found 256.0 $[M+H]^+$, 278.0 $[M+Na]^+$.

4.8. General procedure for synthesis of 4-chloro-2-(alkyl or arylalkyl)-2*H*-pyrazolo[3,4-*d*]pyrimidin-6-amine (31–34)

A mixture of 6-amino-2-(alkyl or arylalkyl)-2*H*-pyrazolo[3,4-*d*]pyrimidin-4(5*H*)-ones (**27**–**30**) (0.005 mol), phosphoroyl trichloride (0.1 mol, 20 equiv) and N–N dimethylamine (0.005 mol, 1 equiv) was refluxed at 110 °C for 24 h. Then the reaction mixture was cooled and the excess phosphoroyl chloride was removed under reduced pressure. The resulting red oil was poured onto ice mixture slowly, stirred for 10 min and the aqueous part was extracted with EtOAc (3 × 10 mL). The combined organic layers were dried over Na_2SO_4, filtered, and the solvent was removed under reduced pressure to give a oily residue that was purified via column chromatography eluting with a mixture of hexane/ethyl acetate (5:5) to obtain pale yellow solids as desired products **(31–34)**.

4.8.1. 4-Chloro-2-methyl-2*H*-pyrazolo[3,4-*d*]pyrimidin-6-amine (31)

Pale yellow solid: Yield (0.536 g, 65%); mp 247–249 °C. HPLC purity (254 nm); 98.2%, eluent: 60% ACN/H_2O, t_R = 2.2 min.

4.8.2. 4-Chloro-2-isopropyl-2*H*-pyrazolo[3,4-*d*]pyrimidin-6-amine (32)

Pale yellow solid: Yield (0.647 g, 67 %); mp 151–153 °C. ^{1}H NMR (400 MHz, DMSO-d_6): δ 1.48 (d, J = 6.64 Hz, 6H, $2CH_3$), 4.53 (sep, J = 6.52 Hz, 1H, CH), 6.18 (s, 2H, NH_2), 8.30 (s, 1H, pyrazole-H). ^{13}C NMR (400 MHz, DMSO-d_6): δ22.0 (CH_3), 48.4 (CH-alkyl), 106.7 (C), 132.1 (CH-pyrazole), 153.7 (C–Cl), 155.1 (C–NH_2), 166.6 (N–C–N–). LC–MS (ESI) analysis (*m*/*z*) calcd for $C_8H_{10}ClN_5$ (211.65): found 212.1 $[M+H]^+$, HPLC purity (254 nm); 96.8%, eluent: 60% ACN/H_2O, t_R = 3.3 min.

4.8.3. 4-Chloro-2-neopentyl-2*H*-pyrazolo[3,4-*d*]pyrimidin-6-amine (33)

Pale yellow solid: Yield (0.815 g, 77%); mp 154–156 °C. ^{1}H NMR (400 MHz, DMSO-d_6): δ 0.96 (s, 9H, $3CH_3$), 4.01 (s, 2H, CH_2), 7.29 (s, 2H, NH_2), 8.02 (s, 1H, pyrazole-H).^{13}C NMR (400 MHz, DMSO-d_6): δ 28.1 (CH_3), 33.7 (C-Alkyl), 57.3 (CH_2), 106.2 (C), 132.2 (CH-pyrazole), 153.9 (C–Cl), 156.9 (C–NH_2), 161.8 (N–C–N–). LC–MS (ESI) analysis (*m*/*z*) calcd for $C_{10}H_{14}ClN_5$ (239.70): found 240.0$[M+H]^+$. HPLC purity (254 nm); 100%, eluent: 60% ACN:H_2O, t_R = 6.0 min.

4.8.4. 4-Chloro-2-phenethyl-2*H*-pyrazolo[3,4-*d*]pyrimidin-6-amine (34)

Pale yellow solid: Yield (0.918 g, 72%); mp 146–148 °C. ^{1}H NMR (400 MHz, DMSO-d_6): δ 3.10 (t, J = 6.95 Hz, 2H, CH_2), 4.38 (t, J = 7.55 Hz, 2H, CH_2), 7.10–7.22 (m, 5H, Ar-H), 7.26 (s, 2H, NH_2), 7.97 (s,1H, pyrazole-H). ^{13}C NMR (400 MHz, DMSO-d_6): δ 35.0 (CH_2), 47.8 (N–CH_2), 106.5 (C), 126.8 (CH), 128.8 (CH), 129.0 (CH), 132.4 (CH), 138.6 (CH-pyrazole), 153.8 (C–Cl), 156.1 (C–NH_2), 161.7 (N–C–N–). LC–MS (ESI) analysis (*m*/*z*) calcd for $C_{13}H_{12}ClN_5$ (273.72): found 272.0 $[M-H]^+$. HPLC purity (254 nm); 99.3%, eluent: 60% ACN/H_2O, t_R = 5.5 min.

4.9. General procedure for synthesis of 6-amino-2-neopentyl-2*H*-pyrazolo[3,4-*d*]pyrimidine-4-carbonitrile (35)

A mixture of 4-chloro-2-neopentyl-2*H*-pyrazolo[3,4-*d*]pyrimidin-6-amine **33** (0.00054 mol), sodium cyanide (0.0011 mol, 2 equiv), sodium *p*-toluene sulfinate (0.00016 mol, 0.3 equiv) in 5 mL of anhydrous DMF was heated on an oil bath at 80 °C for 2 h. The resultant mixture was cooled, poured into ice water mixture and stirred for 10 min. The solid was collected by filtration, washed with water and recrystallized from dimethylformamide and methanol mixture to obtain the desired products (**35)** as solids.

Yield: 62%; pale yellow solid, mp 148–150 °C; ^{1}H NMR (400 MHz, DMSO-d_6): δ 0.98 (s, 9H, $3CH_3$), 4.06 (s, 2H, CH_2), 7.48 (s, 2H, NH_2), 8.27 (s, 1H, pyrazole-H).^{13}C NMR (400 MHz, DMSO-d_6): δ 28.1 (CH_3), 33.7 (C), 57.2 (CH_2), 108.5 (C), 115.1(CN), 131.8 (CH-pyrazole), 135.4 (C–CN), 156.6 (C–NH_2), 162.3 (N–C–N–). LC–MS (ESI) analysis (*m*/*z*) calcd for $C_{11}H_{14}N_6$ (230.27): found 229.2 $[M-H]^+$.

4.10. General procedure for synthesis of 6-amino-2-neopentyl-2*H*-pyrazolo[3,4-*d*]pyrimidine-4-carboxamide (36)

To a stirred solution of 6-amino-2-neopentyl-2*H*-pyrazolo[3,4-*d*]pyrimidine-4-carbonitrile **35** (0.00057 mol) in DMSO (3 mL) at cold condition, 30% H_2O_2 (0.0023 mol, 4 equiv) and anhydrous K_2CO_3 (0.0011 mol, 2 equiv) were added. The mixture was stirred at room temperature for 1 h. Then the resultant mixture was poured into ice water mixture and stirred for 10 min. The solid was collected by filtration, washed with water and recrystallized from methanol to obtain the desired products (**36)** as solids.

Yield: 79%; White solid, mp 174–176 °C; ^{1}H NMR (DMSO-d_6): δ 0.99 (s, 9H, $3CH_3$), 4.07 (s, 2H, CH_2), 7.03 (s, 2H, NH_2), 7.89 (br s, 1H, NH), 8.00 (br s, 1H, NH), 8.24 (s, 1H, pyrazole-H). LC–MS (ESI) analysis (*m*/*z*) calcd for $C_{11}H_{16}N_6O$ (248.28) : found 247.0 $[M-H]^+$.

4.11. General procedure for synthesis of ethyl-6-amino-2-neopentyl-2*H*-pyrazolo[3,4-*d*]pyrimidine-4-carboxylate (37)

To a solution of 6-amino-2-(alkyl or aralkyl)-2*H*-pyrazolo[3,4-*d*]pyrimidine-4-carboxamides **36** (0.00052 mol) in absolute ethanol (30 mL), conc. H_2SO_4 (3 mL) was added slowly and the resulting mixture was refluxed at 80 °C for 12 h. The reaction mixture was cooled and excess ethanol was evaporated and the resulting oily residue was poured into ice water mixture, stirred for 10 min. The solid was collected by filtration, washed with water and recrystallized from methanol to obtain the desired products (**37)** as solids.

Yield: 84%; pale yellow solid, mp 120–122 °C; ^{1}H NMR (DMSO-d_6): δ 0.99 (s, 9H, $3CH_3$), 1.43 (t, J = 7.0 Hz, 3H, CH_3), 4.07 (s, 2H, CH_2), 4.47 (q, J_1 = 7.0 Hz, J_2 = 14.18 Hz, 2H, $COOCH_2$), 7.27 (s, 2H, NH_2), 8.18 (s, 1H, pyrazole-H). ^{13}C NMR (400 MHz, DMSO-d_6): δ 14.5 (CH_3), 28.2 (CH_3)$_3$, 33.8 (C), 57.0 (CH_2), 62.3 ($COOCH_2$), 106.0 (C), 133.7 (CH-pyrazole), 151.0 (C–COO), 157.7 (C–NH_2), 162.7 (N–C–N–), 163.9 (COO). LC–MS (ESI) analysis (*m*/*z*) calcd for $C_{13}H_{19}N_5O_2$ (277.32): found 278.3 $[M+H]^+$, 300.2 $[M+Na]^+$. HPLC purity (254 nm); 97.9 %, eluent: 60% ACN/H_2O, t_R = 3.6 min.

4.12. General procedure for synthesis of *N*-(4-chloro-2(alkyl or arylalkyl)-2*H*-pyrazolo[3,4-*d*]pyrimidin-6-yl) benzamide (38–41, 42–45, 46–49, 50–53)

To a suspension of 4-chloro-2-(alkyl or arylalkyl)-2*H*-pyrazolo[3,4-*d*]pyrimidin-6-amines **31**–**34** (0.001 mol) in toluene,

diisopropylethylamine (0.002 mol, 2 equiv) and benzoyl chloride or substituted benzoyl chlorides (0.002 mol, 2 equiv) were added. The mixture was heated under reflux at 120 °C for 24 h. The solvent was removed under reduced pressure and the resulting residue was purified by column chromatography (hexane/EtOAc, 5:5).

4.12.1. *N*-(4-Chloro-2-methyl-2*H*-pyrazolo[3,4-*d*]pyrimidin-6-yl)benzamide (38)

White solid: Yield (0.066 g, 36%); mp 165–167 °C. ^{1}H NMR (400 MHz, DMSO-d_6): δ 3.99 (s, 3H, N–CH_3), 7.51–7.64 (m, 3H, Ar-H), 7.99 (d, J = 7.52 Hz, 2H, Ar-H), 8.34 (s, 1H, pyrazole-H), 11.42 (s, 1H, NH). LC–MS (ESI) analysis (m/z) calcd for $C_{13}H_{10}ClN_5O$ (287.70): found 288.1 $[M+H]^+$, 310.1 $[M+Na]^+$. HPLC purity (254 nm); 97.8%, eluent: 60% ACN:H_2O, t_R = 2.9 min.

4.12.2. *N*-(4-Chloro-2-methyl-2*H*-pyrazolo[3,4-*d*]pyrimidin-6-yl)-4-fluorobenzamide (39)

White solid: Yield (0.0786 g, 43%); mp 140–142 °C. ^{1}H NMR (400 MHz, DMSO-d_6): δ 3.98 (s, 3H, N–CH_3), 7.33–7.37 (m, 2H, Ar-H), 8.05–8.09 (m, 2H, Ar-H), 8.35 (s, 1H, pyrazole-H), 11.46 (s, 1H, NH). LC–MS (ESI) analysis (m/z) calcd for $C_{21}H_{18}ClN_5O$ (391.85): found 392.0 $[M+H]^+$. HPLC purity (254 nm); 99.4%, eluent: 60% ACN/H_2O, t_R = 3.3 min.

4.12.3. *N*-(4-Chloro-2-methyl-2*H*-pyrazolo[3,4-*d*]pyrimidin-6-yl)-4-(trifluoromethyl)benzamide (40)

White solid: Yield (0.104 g, 57%); mp 145–147 °C. ^{1}H NMR (400 MHz, DMSO-d_6): δ 3.98 (s, 3H, N–CH_3), 7.88-7.90 (m, 2H, Ar-H), 8.16–8.17 (m, 2H, Ar-H), 8.35 (s, 1H, pyrazolo-H), 11.67 (s, 1H, NH). LC–MS (ESI) analysis (m/z) calcd for $C_{14}H_9ClF_3N_5O$ (355.70): found 356.2 $[M+H]^+$, 378.2 $[M+Na]^+$. HPLC purity (254 nm); 99.8%, eluent: 60% ACN:H_2O, t_R = 5.7 min.

4.12.4. *N*-(4-Chloro-2-methyl-2*H*-pyrazolo[3,4-*d*]pyrimidin-6-yl)-4-methylbenzamide (41)

White solid: Yield (0.0768 g, 42%); mp 149–151 °C. ^{1}H NMR (400 MHz, DMSO-d_6): δ 2.39 (s, 3H, CH_3), 3.98 (s, 3H, N–CH_3), 7.31–7.92 (m, 4H, Ar-H), 8.33 (s, 1H, pyrazole-H), 11.32 (s, 1H, NH). LC–MS (ESI) analysis (m/z) calcd for $C_{14}H_{12}ClN_5O$ (301.73): found 302.0 $[M+H]^+$. HPLC purity (254 nm); 99.4%, eluent: 60% ACN/H_2O, t_R = 3.8.

4.12.5. *N*-(4-Chloro-2-isopropyl-2*H*-pyrazolo[3,4-*d*]pyrimidin-6-yl)benzamide (42)

White solid: Yield (0.059 g, 28%); mp 151–153 °C. ^{1}H NMR (400 MHz, DMSO-d_6): δ 1.50 (d, J = 6.76 Hz, 6H, 2CH_3), 5.01 (sep, J = 6.52 Hz, 1H, CH), 7.50–7.99 (m, 5H, Ar-H), 8.35 (s, 1H, pyrazole-H), 11.39 (s, 1H, NH). LC–MS (ESI) analysis (m/z) calcd for $C_{15}H_{14}ClN_5O$ (315.76): found 316.2 $[M+H]^+$, 338.3 $[M+Na]^+$. HPLC purity (254 nm); 100%, eluent: 60% ACN/H_2O, t_R = 4.2.

4.12.6. *N*-(4-Chloro-2-isopropyl-2*H*-pyrazolo[3,4-*d*]pyrimidin-6-yl)-4-fluorobenzamide (43)

White solid: Yield (0.0846 g, 40 %); mp 120–122 °C. ^{1}H NMR (400 MHz, DMSO-d_6): δ 1.51 (d, J = 6.76 Hz, 6H, 2CH_3), 5.02 (sep, J = 6.76 Hz, 1H, CH), 7.46–7.85 (m, 4H, Ar-H), 8.36 (s, 1H, pyrazole-H), 11.49 (s, 1H, NH). LC–MS (ESI) analysis (m/z) calcd for $C_{15}H_{13}ClFN_5O$ (333.75): found 334.2 $[M+H]^+$, 356.3 $[M+Na]^+$. HPLC purity (254 nm); 100%, eluent: 60% ACN/H_2O, t_R = 4.6 min.

4.12.7. *N*-(4-Chloro-2-isopropyl-2*H*-pyrazolo[3,4-*d*]pyrimidin-6-yl)-4-(trifluoromethyl)benzamide (44)

White solid: Yield (0.0842 g, 38 %); mp 146–148 °C. ^{1}H NMR (400 MHz, DMSO-d_6): δ 1.47 (d, J = 6.8 Hz, 6H, 2CH_3), 4.96 (sep, J = 6.64 Hz, 1H, CH), 7.86–8.15 (m, 4H, Ar-H), 8.35 (s, 1H, pyrazole-H), 11.65 (s, 1H, NH). LC–MS (ESI) analysis (m/z) calcd for $C_{16}H_{13}ClF_3N_5O$ (383.76): found 384.2 $[M+H]^+$, 406.2 $[M+Na]^+$. HPLC purity (254 nm); 99.6%, eluent: 60% ACN/H_2O, t_R = 7.3 min.

4.12.8. *N*-(4-Chloro-2-isopropyl-2*H*-pyrazolo[3,4-*d*]pyrimidin-6-yl)-4-methylbenzamide (45)

White solid: Yield (0.0719 g, 34%); mp 131–133 °C. ^{1}H NMR (400 MHz, DMSO-d_6): δ 1.50 (d, , J = 6.64 Hz, 6H, 2CH_3), 2.39 (s, 3H, CH_3), 5.00 (sep, J = 6.64 Hz, 1H, CH), 7.32 (d, J = 8.04 Hz, 2H, Ar-H), 7.91 (d, J = 8.12 Hz, 2H, Ar-H), 8.34 (s, 1H, pyrazole-H), 11.31 (s, 1H, NH). LC–MS (ESI) analysis (m/z) calcd for $C_{16}H_{16}ClN_5O$ (329.78): found 330.2 $[M+H]^+$, 352.1 $[M+Na]^+$. HPLC purity (254 nm); 95.7%, eluent: 60% ACN/H_2O, t_R = 5.2 min.

4.12.9. *N*-(4-Chloro-2-neopentyl-2*H*-pyrazolo[3,4-*d*]pyrimidin-6-yl)benzamide (46)

White solid: Yield (0.105 g, 44%); mp 135–137 °C. ^{1}H NMR (400 MHz, DMSO-d_6): δ 0.95 (s, 9H, 3CH_3), 4.16 (s, 2H, CH_2), 7.51–8.0 (m, 5H, Ar-H), 8.38 (s, 1H, pyrazole-H), 11.38 (s, 1H, NH). LC–MS (ESI) analysis (m/z) calcd for $C_{17}H_{18}ClN_5O$ (343.81): found 344.2 $[M+H]^+$, 366.3 $[M+Na]^+$. HPLC purity (254 nm); 97.8%, eluent: 60% ACN/H_2O, t_R = 7.2 min.

4.12.10. *N*-(4-Chloro-2-neopentyl-2*H*-pyrazolo[3,4-*d*]pyrimidin-6-yl)-4-fluorobenzamide (47)

White solid: Yield (0.129 g, 54%); mp 132–134 °C. ^{1}H NMR (400 MHz, DMSO-d_6): δ 0.95 (s, 9H, 3CH_3), 4.15 (s, 2H, CH_2), 7.33–8.05 (m, 4H, Ar-H), 8.37 (s, 1H, pyrazole-H), 11.42 (s, 1H, NH). LC–MS (ESI) analysis (m/z) calcd for $C_{17}H_{17}ClFN_5O$ (361.80): found 362.2 $[M+H]^+$, 384.2 $[M+Na]^+$. HPLC purity (254 nm); 98.3%, eluent: 60% ACN/H_2O, t_R = 8.0 min.

4.12.11. *N*-(4-Chloro-2-neopentyl-2*H*-pyrazolo[3,4-*d*]pyrimidin-6-yl)-4-(trifluoromethyl)benzamide (48)

White solid: Yield (0.0935 g, 39%); mp 129–131 °C. ^{1}H NMR (400 MHz, DMSO-d_6): δ 0.92 (s, 9H, 3CH_3), 4.10 (s, 2H, CH_2), 7.87–8.13 (m, 4H, Ar-H), 8.38 (s, 1H, pyrazole-H), 11.63 (s, 1H, NH). LC–MS (ESI) analysis (m/z) calcd for $C_{18}H_{17}ClF_3N_5O$ (411.81): found 412.3 $[M+H]^+$, 434.3 $[M+Na]^+$. HPLC purity (254 nm); 95.4%, eluent: 60% ACN/H_2O, t_R = 10.9 min.

4.12.12. *N*-(4-Chloro-2-neopentyl-2*H*-pyrazolo[3,4-*d*]pyrimidin-6-yl)-4-methylbenzamide (49)

White solid: Yield (0.0839 g, 35%); mp 134–136 °C. ^{1}H NMR (400 MHz, DMSO-d_6): δ 0.94 (s, 9H, 3CH_3), 2.36 (s, 3H, CH_3), 4.15 (s, 2H, CH_2), 7.28–7.89 (m, 4H, Ar-H), 8.34 (s, 1H, pyrazole-H), 11.28 (s, 1H, NH). LC–MS (ESI) analysis (m/z) calcd for $C_{18}H_{20}ClN_5O$ (357.84): found 358.3 $[M+H]^+$, 380.2 $[M+Na]^+$. HPLC purity (254 nm); 98.4%, eluent: 60% ACN/H_2O, t_R = 8.3 min.

4.12.13. *N*-(4-Chloro-2-phenethyl-2*H*-pyrazolo[3,4-*d*]pyrimidin-6-yl) benzamide (50)

White solid: Yield (0.123 g, 45%); mp 140–142 °C. ^{1}H NMR (400 MHz, DMSO-d_6): δ 3.23 (t, J = 7.28 Hz, 2H, CH_2), 4.60 (t, J = 7.04 Hz, 2H, CH_2), 7.17–7.26 (m, 5H, Ar-H), 7.51–8.00 (m, 5H, acyl-H), 8.34 (s, 1H, pyrazole-H), 11.38 (s, 1H, NH). LC–MS (ESI) analysis (m/z) calcd for $C_{20}H_{16}ClN_5O$ (377.83): found 378.3 $[M+H]^+$, 400.2 $[M+Na]^+$. HPLC purity (254 nm); 99.7%, eluent: 60% ACN/H_2O, t_R = 6.7 min.

4.12.14. *N*-(4-Chloro-2-phenethyl-2*H*-pyrazolo[3,4-*d*]pyrimidin-6-yl)-4-fluorobenzamide (51)

White solid: Yield (0.101 g, 37%); mp 127–129 °C. ^{1}H NMR (400 MHz, DMSO-d_6): δ 3.23 (t, J = 7.44 Hz, 2H, CH_2), 4.61 (t, J = 7.04 Hz, 2H, CH_2), 7.15–7.19 (m, 5H, Ar-H), 7.22–7.26 (m, 2H, CH), 8.05–8.08 (m, 2H, CH), 8.34 (s, 1H, pyrazole-H), 11.43 (s, 1H, NH). LC–MS (ESI) analysis (m/z) calcd for $C_{20}H_{15}ClFN_5O$ (395.82):

found 396.3 $[M+H]^+$, 418.3 $[M+Na]^+$. HPLC purity (254 nm); 99.6%, eluent: 60% ACN/H_2O, t_R = 7.3 min.

4.12.15. *N*-(4-Chloro-2-phenethyl-2*H*-pyrazolo[3,4-*d*]pyrimidin-6-yl)-4-(trifluoromethyl)benzamide (52)

White solid: Yield (0.139 g, 51%); mp 137–139 °C. ^1H NMR (400 MHz, DMSO-d_6): δ 3.20 (t, J = 7.28 Hz, 2H, CH_2), 4.59 (t, J = 7.16 Hz, 2H, CH_2), 7.16–7.25 (m, 5H, Ar-H), 7.86–8.15 (m, 5H, acyl-H), 8.34 (s, 1H, pyrazole-H), 11.63 (s, 1H, NH). LC–MS (ESI) analysis (m/z) calcd for $C_{21}H_{15}ClF_3N_5O$ (445.82): found 446.3 $[M+H]^+$, 468.2 $[M+Na]^+$. HPLC purity (254 nm); 98.7%, eluent: 60% ACN:H_2O, t_R = 9.2 min.

4.12.16. *N*-(4-Chloro-2-phenethyl-2*H*-pyrazolo[3,4-*d*]pyrimidin-6-yl)-4-methylbenzamide (53)

White solid: Yield (0.109 g, 40 %); mp 131–133 °C. ^1H NMR (400 MHz, DMSO-d_6): δ 2.39 (s, 3H, CH_3), 3.22 (t, J = 7.16 Hz, 2H, CH_2), 4.60 (t, J = 7.04 Hz, 2H, CH_2), 7.17–7.25 (m, 5H, Ar-H), 7.25–7.91 (m, 5H, acyl-H), 8.33 (s, 1H, pyrazole-H), 11.29 (s, 1H, NH). LC–MS (ESI) analysis (m/z) calcd for $C_{21}H_{18}ClN_5O$ (391.85): found 392.0 $[M+H]^+$. HPLC purity (254 nm); 97.6%, eluent: 60% ACN:H_2O, t_R = 6.9 min.

4.13. General procedure for synthesis of *N*-benzoyl-*N*-(4-chloro-2-(alkyl or arylalkyl)-2*H*-pyrazolo[3,4-*d*]pyrimidin-6-yl) benzamide (54–57)

To a suspension of 4-chloro-2-(alkyl or arylalkyl)-2*H*-pyrazolo[3,4-*d*]pyrimidin-6-amines **31**–**34** (0.001 mol) in toluene, diisopropylethylamine (0.004 mol, 4 equiv) and benzoyl chloride (0.004 mol, 4 equiv) were added. The mixture was heated under reflux for 18 h.The solvent was removed under reduced pressure and the resulting residue was purified by column chromatography (hexane/EtOAc, 5:5).

4.13.1. *N*-Benzoyl-*N*-(4-chloro-2-methyl-2*H*-pyrazolo[3,4-*d*]pyrimidin-6-yl)benzamide (54)

White solid: Yield (0.112 g, 61%); mp 163–165 °C. ^1H NMR (DMSO-d_6): δ 3.88 (s, 3H, N–CH_3), 7.53-7.87 (m, 10H, Ar-H), 8.53 (s, 1H, pyrazole-H). LC–MS (ESI) analysis (m/z) calcd for $C_{20}H_{14}ClN_5O_2$ (391.81): found 392.1 $[M+H]^+$. HPLC purity (254 nm); 99.9%, eluent: 60% ACN/H_2O, t_R = 4.5 min.

4.13.2. *N*-Benzoyl-*N*-(4-chloro-2-isopropyl-2*H*-pyrazolo[3,4-*d*]pyrimidin-6-yl)benzamide (55)

White solid: Yield (0.1206 g, 57%); mp 153–155 °C. ^1H NMR (DMSO-d_6): δ 1.21–1.22 (d, J = 6.8 Hz, 6H, $2CH_3$), 4.67–4.74 (sep, 1H, CH), 7.47–7.82 (m, 10H, Ar-H), 8.45 (s, 1H, pyrazole-H). LC–MS (ESI) analysis (m/z) calcd for $C_{22}H_{18}ClN_5O$ (419.86): found 421.3 $[M+H]^+$, 442.3$[M+Na]^+$. HPLC purity (254 nm); 99.4%, eluent: 60% ACN/H_2O, t_R = 7.2 min.

4.13.3. *N*-Benzoyl-*N*-(4-chloro-2-neopentyl-2*H*-pyrazolo[3,4-*d*]pyrimidin-6-yl)benzamide (56)

Yield: 52%; White solid, mp 161–162 °C; ^1H NMR (400 MHz, DMSO-d_6): δ 0.61 (s, 9H, $3CH_3$), 4.01 (s, 2H, CH_2), 7.48–7.83 (m, 10H, Ar-H), 8.52 (s, 1H, pyrazole-H). LC–MS (ESI) analysis (m/z) calcd for $C_{24}H_{22}ClN_5O_2$ (447.92): found 448.1$[M+H]^+$, 470.1$[M+Na]^+$. HPLC purity (254 nm); 100.0%, eluent: 60% ACN/H_2O, t_R = 11.6 min.

4.13.4. *N*-Benzoyl-*N*-(4-chloro-2-phenethyl-2*H*-pyrazolo[3,4-*d*]pyrimidin-6-yl)benzamide (57)

Yield: 46%; White solid, mp 134–135 °C; ^1H NMR (400 MHz, DMSO-d_6): δ 2.79 (t, 7.0 Hz, 3H, CH_3), 4.45 (t, J = 7.04 Hz, 2H, CH_2), 6.86–7.20 (m, 5H, Ar-H), 7.49–7.82 (m, 10H, acyl-H), 8.41 (s, 1H, pyrazole-H). LC–MS (ESI) analysis (m/z) calcd for $C_{27}H_{20}ClN_5O_2$ (481.93): found 482.1$[M+H]^+$, 504.1$[M+Na]^+$. HPLC purity (254 nm); 98.6%, eluent: 60% ACN/H_2O, t_R = 12.3 min.

4.14. General procedure for synthesis of *N*-(4-chloro-2-(alkyl or arylalkyl)-2*H*-pyrazolo[3,4-*d*]pyrimidin-6-yl)-2-phenyl acetamide (58–61)

To a suspension of 4-chloro-2-(alkyl or arylalkyl)-2*H*-pyrazolo[3,4-*d*]pyrimidin-6-amines **31**–**34** (0.001 mol) in toluene, diisopropylethylamine (0.002 mol, 2 equiv) and phenyl acetyl chloride (0.002 mol, 2 equiv) were added. The mixture was heated under reflux for 12 h. Subsequently, another 0.001 mol equivalent of diisopropylethylamine and phenyl acetyl chloride were added and refluxing continued for 12 h again. The solvent was then removed under reduced pressure and the resulting residue was purified by column chromatography (hexane/EtOAc, 5:5).

4.14.1. *N*-(4-Chloro-2-methyl-2*H*-pyrazolo[3,4-*d*]pyrimidin-6-yl)-2-phenylacetamide (58)

White solid: Yield (0.0771 g, 42%); mp 147–149 °C. ^1H NMR (DMSO-d_6): δ 3.83 (s, 2H, CH_2), 3.94 (s, 3H, N–CH_3), 7.24–7.34 (m, 5H, Ar-H), 8.30 (s, 1H, pyrazole-H), 11.23 (s, 1H, NH). LC–MS (ESI) analysis (m/z) calcd for $C_{14}H_{12}ClN_5O$ (301.73): found 302.0 $[M+H]^+$. HPLC purity (254 nm); 96.2%, eluent: 60% ACN/H_2O, t_R = 4.2 min.

4.14.2. *N*-(4-Chloro-2-isopropyl-2*H*-pyrazolo[3,4-*d*]pyrimidin-6-yl)-2-phenylacetamide (59)

White solid: Yield (0.0910 g, 43%); mp 146–148 °C. ^1H NMR (DMSO-d_6): δ 1.47 (d, J = 6.76 Hz, 6H, $2CH_3$), 3.83 (s, 2H, CH_2), 4.94–4.98 (sep, J = 6.64 Hz, 1H, CH), 7.24–7.35 (m, 1H, CH), 8.30 (s, 1H, pyrazole-H), 11.21 (s, 1H, NH). LC–MS (ESI) analysis (m/z) calcd for $C_{16}H_{16}ClN_5O$ (329.78): found 330.0 $[M+H]^+$, 352.3 $[M+Na]^+$. HPLC purity (254 nm); 99.5%, eluent: 60% ACN:H_2O, t_R = 5.3 min.

4.14.3. *N*-(4-Chloro-2-neopentyl-2*H*-pyrazolo[3,4-*d*]pyrimidin-6-yl)-2-phenylacetamide (60)

White solid: Yield (0.1078 g, 45%); mp 155–157 °C. ^1H NMR (DMSO-d_6): δ 0.93 (s, 9H, $3CH_3$), 3.85 (s, 2H, CH_2 Ar), 4.12 (s, 2H, CH_2), 7.24–7.34 (m, 5H, Ar-H), 8.33 (s, 1H, pyrazole-H), 11.19 (s, 1H, NH). LC–MS (ESI) analysis (m/z) calcd for $C_{18}H_{20}ClN_5O$ (357.84): found 358.1 $[M+H]^+$, 380.5 $[M+Na]^+$. HPLC purity (254 nm); 98.3%, eluent: 60% ACN/H_2O, t_R = 10.0 min.

4.14.4. *N*-(4-Chloro-2-phenethyl-2*H*-pyrazolo[3,4-*d*]pyrimidin-6-yl)-2-phenylacetamide (61)

White solid: Yield (0.1067 g, 39 %); mp 141–143 °C. ^1H NMR (DMSO-d_6): δ 3.20 (t, J = 7.16 Hz, 2H, CH_2), 3.85 (s, 2H, CH_2), 4.57 (t, J = 6.88 Hz, 2H, CH_2), 7.12–7.21 (m, 5H, Ar-H), 7.25–7.34 (m, 5H, Ar-H), 8.30 (s,1H, pyrazole-H), 11.17 (s, 1H, NH). LC–MS (ESI) analysis (m/z) calcd for $C_{21}H_{18}ClN_5O$ (391.85): found 392.3 $[M+H]^+$, 414.0 $[M+Na]^+$. HPLC purity (254 nm); 99.5%, eluent: 60% ACN/H_2O, t_R = 7.9 min.

4.15. General procedure for synthesis of ethyl 6-benzamido-neopentyl-2*H*-pyrazolo[3,4-*d*]pyrimidine-4-carboxylate (62 & 63)

To a suspension of ethyl 6-amino-2-(neopentyl)-2*H*-pyrazolo[3,4-*d*]pyrimidine-4-carboxylates **37** (0.00045 mol) in anhydrous toluene (5 mL), diisopropylethylamine (0.00135 mol, 3 equiv) and substituted benzoyl chlorides (0.00135 mol, 3 equiv) were added. The mixture was heated under reflux for 24 h. The solvent was removed under reduced pressure and the resulting residue was

purified by column chromatography (hexane/EtOAc, 4:6) to obtain the desired products (**62** & **63**) as solids.

4.15.1. Ethyl-2-neopentyl-6-(4-(trifluoromethyl)benzamido)-2*H*-pyrazolo[3,4-*d*]pyrimidine-4-carboxylate (62)

Yield: 61%; pale yellow solid, mp 116–118 °C; ^{1}H NMR (400 MHz, DMSO-d_6): δ 0.99 (s, 9H, $3CH_3$), 1.47 (t, J = 7.0 Hz, 3H, CH_3), 4.20 (s, 2H, CH_2), 4.55 (q, J_1 = 7.02 Hz, J_2 = 14.18 Hz, 2H, CH_2), 7.93–8.20 (m, 4H, Ar-H), 8.53 (s, 1H, pyrazole-H), 11.76 (s, 1H, NH). LC–MS (ESI) analysis (m/z) calcd for $C_{21}H_{22}F_3N_5O_3$ (449.43) : found 450.4 $[M+H]^+$, 472.2 $[M+Na]^+$. HPLC purity (254 nm); 100%, eluent: 60% ACN:H_2O, t_R = 7.9 min.

4.15.2. Ethyl-6-(4-methylbenzamido)-2-neopentyl-2*H*-pyrazolo[3,4-*d*]pyrimidine-4-carboxylate (63)

Yield: 48%; pale yellow solid, mp 97–99 °C; ^{1}H NMR (400 MHz, DMSO-d_6): δ 1.01 (s, 9H, $3CH_3$), 1.48 (t, J = 7.16 Hz, 3H, CH_3), 2.45 (s, 3H, CH_3), 4.25 (s, 2H, CH_2), 4.55 (q, J_1 = 7.16 Hz, J_2 = 14.16 Hz, 2H, CH_2), 7.36–7.98 (m, 4H, Ar-H), 8.51 (s,1H, pyrazole-H), 11.39 (s, 1H, NH). ^{13}C NMR (400 MHz, DMSO-d_6): δ 14.5 (CH_3), 21.5 (CH_3), 28.1 $(CH_3)_3$, 33.8 (C-alkyl), 57.8 (CH_2), 62.7 ($COOCH_2$), 109.4 (C), 128.9 (CH), 129.3 (CH), 129.9 (C), 131.7 (C), 133.9 (CH-pyrazole), 142.8 (N–C–N), 150.9 (C–COO), 156.3 (C–NH), 163.5 (CO), 166.3 (COO). LC–MS (ESI) analysis (m/z) calcd for $C_{21}H_{25}N_5O_3$ (395.45): found 396.3 $[M+H]^+$, 418.3 $[M+Na]^+$. HPLC purity (254 nm); 100%, eluent: 60% ACN/H_2O, t_R = 7.1 min.

4.16. X-ray diffraction studies

X-ray data were collected with a Bruker AXSSMART APEX diffractometer using MoKa radiation at 223(2) K with the SMART suite of Programs.[44] Data were processed and corrected for Lorentz and polarization effects by means of SAINT software,[45] and for absorption effects using the SADABS software.[46] Structural solution and refinement were carried out by using the SHELXTL suite of programs.[47] The structure was solved by using Direct Methods. Non-hydrogen atoms were located by using difference maps and were given anisotropic displacement parameters in the final refinement. All the H atoms were put at calculated positions by means of the riding model. CCDC-937929 contains the supplementary crystallographic data for this paper. These data can be obtained free of charge from The Cambridge Crystallographic Data Centre via www.ccdc.cam.ac.uk/data_request/cif.

4.17. Binding assay and adenylyl cyclase activity assay

Binding experiments with respective tritiated radioligands at hA_1AR, $hA_{2A}AR$ and hA_3AR were carried out for 3 h at room temperature as described previously.[48] Nonspecific binding was determined in the presence of 1 mM theophylline for hA_1AR and 100 μM (R)-N^6-phenyliso-propyladenosine (R-PIA) for both hA_{2A}-AR and hA_3AR. Bound and free radioactivity was separated by filtering the assay mixture through Whatman GF/B glass-fiber filters using a Micro-Mate 196-cell harvester (Packard Instrument Company). The filter bound radioactivity was counted on Top Count (efficiency of 57%) with Micro-Scint 20. The K_i values were calculated from competition curves by nonlinear curve fitting with the program SCTFIT.[48] In the case of $hA_{2B}AR$, adenylyl cyclase experiments were carried out as described previously with minor modifications.[33,34] Membranes transfected with hA_{2B} receptor were incubated with 100 nM NECA, as well as 150,000 cpm of [α-^{32}P]ATP and tested compounds in different concentrations for 20 min in the incubation mixture without EGTA (ethylene glycol-tetraacetic acid) and NaCl. The K_i values for concentration-dependent inhibition of NECA-mediated adenylyl cyclase activity caused by tested antagonists were calculated accordingly.

4.18. Computational methodologies

All modeling studies were carried out on a Intel(R) Core[TM] 2 Quad CPU Q9550, 2.83 GHz, 3.25 GB RAM, DELL system. Docking simulation, energy calculation and the analyses of docking poses were performed using the Molecular Operating Environment (MOE, version 2010.10) suite.[49] The software package MOPAC (version 7),[50] implemented in the MOE suite, was utilized for all quantum mechanical calculations. PyMOL molecular graphics system was used for graphical visualizations and manipulations.[51]

4.18.1. Homology modeling

The crystallographic structure of human A_{2A} adenosine receptor complexed with ZM-241385 as high affinity antagonist (PDB code: 3EML),[36] was employed to build up a homology model of the hA_3-AR by using software Modeller version 9.11.[37–40] The tip of the second extracellular loop (Gln148 to Ser156) is absent in the crystal structure of $A_{2A}AR$ (PDB No. 3EML) and it was not modelled owing to weak experimental electron density. Such missing tip of the loop is spatially distinct from the ligand-binding site and most probably does not directly interact with the binding cavity, as reported in Jaakola et.al.[36] The refined model was validated using PROCHECK program in Protein Structure Validation Suite[52] (PSVS). The numbering of the amino acids follows the arbitrary scheme as proposed by Ballesteros and Weinstein. According to this scheme, each amino acid identifier starts with the helix number, followed by the position relative to a reference residue among the most conserved amino acid in that helix. The number 50 is arbitrarily assigned to the reference residue.[53]

4.18.2. Molecular docking simulations

Ligand structures were built using MOE-builder tool,[49] and were subjected to MMFF94x energy minimization until the rms of conjugate gradient was <0.05 kcal mol^{-1} Å^{-1}. Partial charges for the ligands were calculated using PM3/ESP methodology.

All ligands were docked into the hypothetical TM binding site of the hA_3AR model and that of the $hA_{2A}AR$ crystal structure by using the docking tool of the MOE suite.[49] In the MOE-Dock, the Alpha PMI placement method, followed by force field refinement and london dG scoring, were used for the docking runs. MOE-Dock performed 100 independent docking runs (100 for our specific case) and wrote the resulting conformations and their energies in a molecular database file. The resulting docked complexes were subjected to MMFF94x energy minimization until the rms of conjugate gradient was <0.1 kcal mol^{-1} Å^{-1}. Prediction of antagonist–receptor complex stability (in terms of corresponding pK_i value) and the quantitative analysis for non bonded intermolecular interactions (H-bonds, hydrophobic, electrostatic) were calculated and visualized using tools implemented in MOE suite.[49] Electrostatic contributions to the binding energy of individual amino acids have been calculated as implemented in MOE suite.[49]

Acknowledgements

This work was supported by the National University of Singapore, and Singapore Ministry of Education (MOE2009-T2-2-011 and R-398-000-068-112; NUS-FRC R-148-000-129-112 and A*STAR-SERC TSRPiNPB 102 152 0016). The authors would like to thank Sonja Kachler for her assistance and expertise in the pharmacological evaluation of the compounds.

Supplementary data

Supplementary data associated with this article can be found, in the online version, at http://dx.doi.org/10.1016/j.bmc.2014.01.018.

References and notes

1. Fredholm, B. B.; Arslan, G.; Halldner, L.; Kull, B.; Schulte, G.; Wasserman, W. *Naunyn-Schmiedeberg's Arch. Pharmacol.* **2000**, *362*, 364.
2. Jacobson, K. A.; Knutsen, L. J. S. In *Handbook of Experimental Pharmacology*; Abbracchio, M. P., Williams, M., Eds.; Springer: Berlin, 2001; Vol. 151, pp 129–175.
3. Moro, S.; Gao, Z. G.; Jacobson, K. A.; Spalluto, G. *Med. Res. Rev.* **2006**, *26*, 131.
4. Cheong, S. L.; Federico, S.; Venkatesan, G.; Mandel, A. L.; Shao, Y. M.; Moro, S.; Spalluto, G.; Pastorin, G. *Med. Res. Rev.* **2013**, *33*, 235.
5. Gessi, S.; Varani, K.; Merighi, S.; Cattabriga, E.; Iannotta, V.; Leung, E.; Baraldi, P. G.; Borea, P. A. *Mol. Pharmacol.* **2002**, *61*, 415.
6. Gessi, S.; Varani, K.; Merighi, S.; Morelli, A.; Ferrari, D.; Leung, E.; Baraldi, P. G.; Spalluto, G.; Borea, P. A. *Br. J. Pharmacol.* **2001**, *134*, 116.
7. Gessi, S.; Fogli, E.; Sacchetto, V.; Merighi, S.; Varani, K.; Preti, D.; Leung, E.; Maclennan, S.; Borea, P. A. *Arterioscler. Thromb. Vasc. Biol.* **2010**, *30*, 90.
8. Merighi, S.; Varani, K.; Gessi, S.; Cattabriga, E.; Iannotta, V.; Ulouglu, C.; Leung, E.; Borea, P. A. *Br. J. Pharmacol.* **2001**, *134*, 1215.
9. Gessi, S.; Sacchetto, V.; Fogli, E.; Merighi, S.; Varani, K.; Baraldi, P. G.; Tabrizi, M. A.; Leung, E.; Maclennan, S.; Borea, P. A. *Biochem. Pharmacol.* **2010**, *79*, 1483.
10. Jajoo, S.; Mukherjea, D.; Watabe, K.; Ramkumar, V. *Neoplasia* **2009**, *11*, 1132.
11. (a) Jiang, J. L.; van Rhee, A. M.; Chang, L.; Patchornik, A.; Ji, X. D.; Evans, P.; Melman, N.; Jacobson, K. A. *J. Med. Chem.* **1997**, *40*, 2596; (b) Jiang, J. L.; Van Rhee, A. M.; Melman, N.; Ji, X. D.; Jacobson, K. A. *J. Med. Chem.* **1996**, *39*, 4667; (c) Li, A. H.; Moro, S.; Forsyth, N.; Melman, N.; Ji, X. D.; Jacobson, K. A. *J. Med. Chem.* **1999**, *42*, 706; (d) Li, A. H.; Moro, S.; Melman, N.; Ji, X. D.; Jacobson, K. A. *J. Med. Chem.* **1998**, *41*, 3186; (e) VanRhee, A. M.; Jiang, J. L.; Melman, N.; Olah, M. E.; Stiles, G. L.; Jacobson, K. A. *J. Med. Chem.* **1996**, *39*, 2980.
12. (a) Ji, X. D.; Melman, N.; Jacobson, K. A. *J. Med. Chem.* **1996**, *39*, 781; (b) Karton, Y.; Jiang, J. L.; Ji, X. D.; Melman, N.; Olah, M. E.; Stiles, G. L.; Jacobson, K. A. *J. Med. Chem.* **1996**, *39*, 2293; (c) Moro, S.; VanRhee, A. M.; Sanders, L. H.; Jacobson, K. A. *J. Med. Chem.* **1998**, *41*, 46.
13. (a) Van Muijlwijk-Koezen, J. E.; Timmerman, H.; Link, R.; Van der Goot, H.; Ijzerman, A. P. *J. Med. Chem.* **1998**, *41*, 3987; (b) Van Muijlwijk-Koezen, J. E.; Timmerman, H.; Link, R.; Van der Goot, H.; Ijzerman, A. P. *J. Med. Chem.* **1998**, *41*, 3994; (C) Van Muijlwijk-Koezen, J. E.; Timmerman, H.; Van der Goot, H.; Menge, W. M.; Von Drabbe Kunzel, J. F.; De Groote, M.; Ijzerman, A. P. *J. Med. Chem.* **2000**, *43*, 2227.
14. Kim, Y. C.; De Zwart, M.; Chang, L.; Moro, S.; Von Frijtag, J. K.; Künzel, V. F. D.; Melman, N.; IJzerman, A. P.; Jacobson, K. A. *J. Med. Chem.* **1998**, *41*, 2835.
15. Biagi, G.; Bianucci, A. M.; Coi, A.; Costa, B.; Fabbrini, L.; Giorgi, I.; Livi, O.; Micco, I.; Pacchini, F.; Santini, E.; Leonardi, M.; Nofal, F. A.; Salerni, O. L.; Scartoni, V. *Bioorg. Med. Chem.* **2005**, *13*, 4679.
16. Baraldi, P. G.; Tabrizi, M. A.; Preti, D.; Bovero, A.; Fruttarolo, F.; Romagnoli, R.; Zaid, N. A.; Moorman, A. R.; Varani, K.; Borea, P. A. *J. Med. Chem.* **2005**, *48*, 5001.
17. Lenzi, O.; Colotta, V.; Catarzi, D.; Varano, F.; Poli, D.; Filacchioni, G.; Varani, K.; Vincenz, A.; Borea, P. A.; Paoletta, S.; Morizzo, E.; Moro, S. *J. Med. Chem.* **2009**, *52*, 7640.
18. Taliani, S.; La Motta, C.; Mugnaini, L.; Simorini, F.; Salerno, S.; Marini, A. M.; Da Settimo, F.; Cosconati, S.; Cosimelli, B.; Greco, G.; Limongelli, V.; Marinelli, L.; Novellino, E.; Ciampi, O.; Daniele, S.; Trincavelli, M. L.; Martini, C. *J. Med. Chem.* **2010**, *53*, 3954.
19. Baraldi, P. G.; Cacciari, B.; Romagnoli, R.; Spalluto, G.; Moro, S.; Klotz, K. N.; Leung, E.; Varani, K.; Gessi, S.; Merighi, S.; Borea, P. A. *J. Med. Chem.* **2000**, *43*, 4768.
20. Morizzo, E.; Capelli, F.; Lenzi, O.; Catarzi, D.; Varano, F.; Filacchioni, G.; Vincenzi, F.; Varani, K.; Borea, P. A.; Colotta, V.; Moro, S. *J. Med. Chem.* **2007**, *50*, 6596.
21. Poli, D.; Catarzi, D.; Colotta, V.; Varano, F.; Filacchioni, G.; Daniele, S.; Trincavelli, L.; Martini, C.; Paoletta, S.; Moro, S. *J. Med. Chem.* **2011**, *54*, 2102.
22. Cheong, S. L.; Dolzhenko, A. V.; Kachler, S.; Paoletta, S.; Federico, S.; Cacciari, B.; Klotz, K. N.; Moro, S.; Spalluto, G.; Pastorin, G. *J. Med. Chem.* **2010**, *53*, 3361.
23. Lipinski, C. A.; Lombardo, F.; Dominy, B. W.; Feeney, P. J. *Adv. Drug Delivery Rev.* **1997**, *23*, 3.
24. Lipinski, C. A. *J. Pharmacol. Toxicol. Methods* **2000**, *44*, 235.
25. Cheong, S. L.; Dolzhenko, A. V.; Paoletta, S.; Rong Lee, E. P.; Kachler, S.; Federico, S.; Klotz, K. N.; Dolzhenko, A. V.; Spalluto, G.; Moro, S.; Pastorin, G. *Bioorg. Med. Chem.* **2011**, *19*, 6120.
26. Baraldi, P. G.; Cacciari, B.; Moro, S.; Spalluto, G.; Pastorin, G.; Ros, T. D.; Klotz, K. N.; Varani, K.; Gessi, S.; Borea, P. A. *J. Med. Chem.* **2002**, *45*, 770.
27. Paira, P.; Chow, M. J.; Venkatesan, G.; Kosaraju, V. K.; Cheong, S. L.; Klotz, K. N.; Ang, W. H.; Pastorin, G. *Chem. Eur. J.* **2013**, *19*, 8321.
28. Shenlin, H. PCT Int. Appl. WO 2011025927, 2011.
29. Qi, C. PCT Int. Appl. WO 2012030924, 2012.
30. Yamazaki, A.; Kumashiro, I.; Takenishi, T. *J. Org. Chem.* **1967**, *32*, 1825.
31. Frank, S.; Herbert, S. *Helv. Chim. Acta* **1986**, *69*, 1602.
32. Miyashita, A.; Sato, S.; Taido, N.; Tanji, K.; Oishi, E.; Higashino, T. *Chem. Pharm. Bull.* **1990**, *38*, 230.
33. Klotz, K. N.; Hessling, J.; Hegler, J.; Owman, C.; Kull, B.; Fredholm, B. B.; Lohse, M. J. *Naunyn-Schmiedeberg's Arch. Pharmacol.* **1998**, *357*, 1.
34. Klotz, K. N.; Cristalli, G.; Grifantini, M.; Vittori, S.; Lohse, M. J. *J. Biol. Chem.* **1985**, *260*, 14659.
35. Cheng, Y. C.; Prusoff, H. R. *Biochem. Pharmacol.* **1973**, *22*, 3099.
36. Jaakola, V. P.; Griffith, M. T.; Hanson, M. A.; Cherezov, V.; Chien, E. Y. T.; Lane, J. R.; Ijzerman, A. P.; Stevens, R. C. *Science* **2008**, *322*, 1211.
37. Eswar, N.; Marti-Renom, M. A.; Webb, B.; Madhusudhan, M. S.; Eramian, D.; Shen, M.; Pieper, U.; Sali, A. *Curr. Protoc. Protein Sci.*; Wiley, 2007. Chapter 2.
38. Marti-Renom, M. A.; Stuart, A.; Fiser, A.; Sánchez, R.; Melo, F.; Sali, A. *Annu. Rev. Biophys. Biomol. Struct.* **2000**, *29*, 291.
39. Sali, A.; Blundell, T. L. *J. Mol. Biol.* **1993**, *234*, 779.
40. Fiser, A.; Do, R. K.; Sali, A. *Protein Sci.* **2000**, *9*, 1753.
41. Duong, H. T.; Gao, Z. G.; Jacobson, K. A. *Nucleosides, Nucleotides Nucleic Acids* **2005**, *24*, 1507.
42. Martinelli, A.; Tuccinardi, T. *Med. Res. Rev.* **2008**, *28*, 247.
43. Gao, Z. G.; Kim, S. K.; Gross, A. S.; Chen, A.; Blaustein, J. B.; Jacobson, K. A. *Mol. Pharmacol.* **2002**, *63*, 1021.
44. *SMART, version 5.628*; Bruker AXS: Madison, WI, 2001.
45. *SAINT+, version 6.22a*; Bruker AXS: Madison, WI, 2001.
46. Sheldrick, G. W. *SADABS, version 2.10*; University of Gottingen: Gottingen, Germany, 2001.
47. *SHELXTL, version 6.14*, Bruker AXS, Madison, WI, 2000.
48. De Lean, A.; Hancock, A. A.; Lefkowitz, R. J. *Mol. Pharmacol.* **1982**, *21*, 5.
49. *MOE (Molecular Operating Environment), version 2010.10*; Chemical computing group: 1010 Sherbrooke Street West, Suite 910, Montreal, Quebec H3A 2R7, Canada, http://www.chemcomp.com.
50. Stewart, J. J. P. *MOPAC 7*; Fujitsu Limited: Tokyo, 1993.
51. De Lano, W. L. *The PyMOL Molecular Graphics System (2002)*; De Lano Scientific.: San Carlos, CA, USA, http://www.pymol.org.
52. Bhattacharya, A.; Tejero, R.; Montelione, G. T. *Proteins* **2007**, *66*, 778.
53. Ballesteros, J. A.; Weinstein, H. *Methods Neurosci.* **1995**, *25*, 366.